TSUNAMI INUNDATION MAPS OF ANCHOR POINT, KENAI, NINILCHIK, AND TYONEK IN COOK INLET, ALASKA

Elena N. Suleimani, J. Barrett Salisbury, and Dmitry J. Nicolsky

TSUNAMI INUNDATION MAPS OF ANCHOR POINT, KENAI, NINILCHIK, AND TYONEK IN COOK INLET, ALASKA

Elena N. Suleimani, J. Barrett Salisbury, and Dmitry J. Nicolsky

STATE OF ALASKA
Mike Dunleavy, Governor

DEPARTMENT OF NATURAL RESOURCES
John Boyle, Commissioner

DIVISION OF GEOLOGICAL & GEOPHYSICAL SURVEYS
Melanie Werdon, State Geologist and Director

Cover photo. Cook Inlet. Photo: Anthony Picasso.

Contents

Figures

Tables

Appendix

Map Sheets

TSUNAMI INUNDATION MAPS OF ANCHOR POINT, KENAI, NINILCHIK, AND TYONEK IN COOK INLET, ALASKA

Elena N. Suleimani[1], J. Barrett Salisbury[2], and Dmitry J. Nicolsky[1]

Abstract

We evaluate potential tsunami hazards for several communities in lower Cook Inlet, including Anchor Point, Kenai, Ninilchik, and Tyonek, by numerically modeling the extent of inundation from tsunami waves generated by hypothetical earthquakes. We define an updated suite of earthquakes—including Tohoku-style megathrust ruptures and other sources in the eastern part of the Alaska–Aleutian megathrust—to calculate vertical seafloor displacements and model resulting tsunami dynamics. A hypothetical earthquake spanning from Kodiak Island to Prince William Sound with maximum slip distributed between depths of 5 and 22 km (3.1 and 13.7 mi) results in "worst case" tsunami inundation for all communities. If the tsunami arrives at high tide, the maximum predicted overland flow depths in the communities can reach up to 10 m (32.8 ft), and the currents could be as strong as 12 m/sec (23.4 knots). Dangerous wave activity is expected to last for more than 24 hours. Results presented here are intended to provide guidance to local emergency management agencies for tsunami inundation assessment, evacuation planning, and public education to mitigate future tsunami damage.

INTRODUCTION

Subduction of the Pacific plate under the North American plate has resulted in numerous great (M > 8) earthquakes and is the source of locally generated tsunamis in Alaska (Dunbar and Weaver, 2008). During the 20th century, several tsunamis generated by Alaska–Aleutian subduction zone earthquakes have resulted in widespread damage and loss of life in exposed coastal communities across the Pacific Ocean basin (Lander, 1996). In this report, we focus on tsunamis originating in the vicinity of the Alaska Peninsula, Aleutian Islands, and Gulf of Alaska as near-field hazards with the potential to reach Alaska's coastal communities within minutes of an earthquake. Reducing property damage and loss of life is highly dependent on community preparedness.

On March 27, 1964, the largest earthquake ever recorded in North America struck Southcentral Alaska. This moment magnitude (M_W) 9.2 megathrust earthquake, known as the Great Alaska Earthquake (fig. 1), generated the most destructive tsunami in Alaska history and, farther south, impacted the west coast of Canada and the United States, as well as the entire Pacific Basin (Plafker and others, 1969; Kanamori, 1970; Johnson and others, 1996; Lander, 1996; Fine and others, 2018a, 2018b; Rabinovich and others, 2019). The tectonic tsunami caused $10 million in damage to the Canadian Pacific coast and about $20 million in damage and 16 fatalities on the United States west coast. In addition to the major tectonic tsunami generated by ocean-floor displacement in the Gulf of Alaska, numerous local tsunamis were generated

[1] Alaska Earthquake Center, Geophysical Institute, University of Alaska, P.O. Box 757320, Fairbanks, Alaska 99775
[2] Alaska Division of Geological & Geophysical Surveys, 3354 College Road, Fairbanks, Alaska 99709

by landslides in coastal communities (Lander, 1996). Landslide-generated tsunamis arrived almost immediately after the earthquake shaking— some before the shaking even stopped— leaving no time for warning or evacuation. Of the 131 fatalities associated with this earthquake, 122 were caused by tsunami waves (Lander, 1996). Despite this relatively recent M_W 9.2 earthquake, the region still has high potential for future large earthquakes, and it is only a matter of time before another devastating tsunami occurs (Kirby and others, 2013). Thus, estimating the potential flooding of the coastal zone from the next local or distant tsunami

event is an essential component of the preparedness process. Combined with high-resolution continuous global positioning system (GNSS and GPS) measurements and recent paleoseismic studies along the southern Alaska coast, the tsunami disasters of 2004 in Indonesia and 2011 in Japan have helped improve our understanding of complex earthquake source mechanisms. Consequently, we include new potential earthquake sources in our tsunami analysis to develop the worst-case credible tsunami scenarios for Cook Inlet communities. This report does not include subaerial or submarine landslide-generated tsunami events.
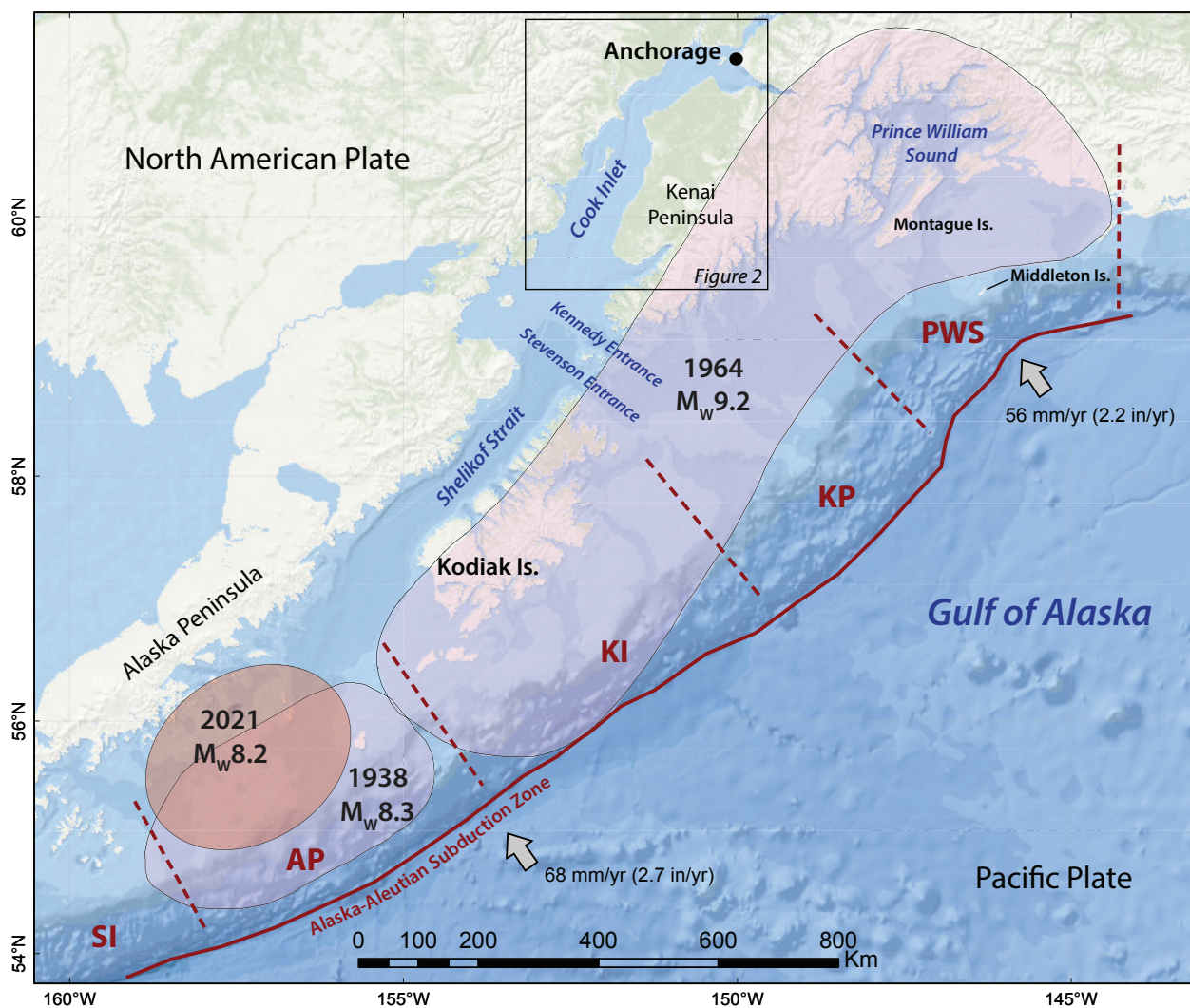
Figure 1. Map of Southcentral Alaska, showing the location of Anchorage and the rupture zones of the 1938, 1964, and 2021 Alaska–Aleutian megathrust earthquakes (shaded areas). SI = Semidi Islands segment, AP = Alaska Peninsula segment, KI = Kodiak Island segment; KP = Kenai Peninsula segment; PWS = Prince William Sound segment.

The tsunami inundation maps for lower Cook Inlet communities described in this report represent the results of a continuous, combined effort of state and federal agencies to mitigate tsunami damage in coastal Alaska. The intended audience of this report is scientists, engineers, emergency managers, and community planners interested in an applied approach to developing tsunami inundation and evacuation maps. Digital data and documentation provided with the report enable technical users to explore the range of possible tsunami inundation for potential events. We use a deterministic approach for our earthquake and tsunami hazard modeling, which is distinctly different from the probabilistic tsunami hazard analysis used in projects with different objectives, such as land-use planning or insurance estimates (Geist and Parsons, 2006). We are less concerned about the probability that an earthquake of a certain magnitude will occur in a given amount of time and are more focused on the community-specific tsunami inundation that might result from the largest hypothetical, yet scientifically plausible earthquake scenarios. The methods used to develop tsunami inundation maps are described in detail in multiple publications and are not reviewed in this report. Refer to Suleimani and others (2016) for a complete description of the process.

PROJECT BACKGROUND: REGIONAL AND HISTORICAL CONTEXT
Setting

Cook Inlet is a major water body in Alaska; it stretches roughly 350 km (220 mi) from the Gulf of Alaska to the Municipality of Anchorage (fig. 1), with an average depth of 100 m (330 ft) and narrowing from 130 to 14 km (80 to 9 mi). At its northern end, Cook Inlet splits into Knik (oriented northeast) and Turnagain (oriented southeast) arms, which surround Anchorage (fig. 2). At its southern entrance, Cook Inlet connects to Shelikof Strait and, through Kennedy and Stevenson entrances, to the Gulf of Alaska. Several glacial-fed

rivers and creeks carry large quantities of sediment into the inlet, forming especially large intertidal mud flats near Anchorage. Importantly, Cook Inlet has extremely large tidal ranges—the largest tidal range in the U.S. is in Turnagain Arm, averaging 9.2 m (30 ft). Tidal fluctuations in the main body of Cook Inlet regularly reach 7 m (23 ft) or higher during the spring tide (Wang and Yang, 2020).

The following information about Cook Inlet communities is from the Alaska Community Database maintained by the State of Alaska, Department of Commerce, Community, and Economic Development, Division of Community and Regional Affairs (DCCED/DCRA, 2015):

Anchor Point, population 2,202, is located on the eastern shore of Cook Inlet on the Kenai Peninsula (fig. 2). It is the westernmost point in the North American highway system. It was given its name in 1778 by Captain James Cook after losing a kedge anchor to the strong tidal currents. A post office was established in 1949.

Kenai, population 7,507, is located on the western coast of the Kenai Peninsula, fronting Cook Inlet (fig. 2). It lies on the western boundary of the Kenai National Wildlife Refuge, on the Kenai Spur Highway. It is approximately 65 air miles and 155 highway miles southwest of Anchorage via the Sterling Highway. In 1957, oil was discovered at Swanson River, 20 miles northeast of Kenai—the first major Alaska oil strike. The city was incorporated in 1960. In 1965, offshore oil discoveries in Cook Inlet fueled a period of rapid growth. Kenai has been a growing center for oil exploration, production, and services since that time.

Ninilchik, population 930, lies on the west coast of the Kenai Peninsula on the Sterling Highway, 38 miles southwest of the City of Kenai and 188 road miles from Anchorage (fig. 2). Ninilchik is a traditional Athabascan village, although most of the population is non-native. The community is unincorporated and has a low population density due to the area's geographic size. Tourism and fishing are the main industries in Ninilchik. There are dozens of

active fishing guides, bed and breakfasts, and other tourism businesses in the area, making it a popular travel destination in the summer.

Tyonek, population 152, lies on the northwest shore of Cook Inlet, 43 miles southwest of Anchorage (fig. 2). Tyonek is a Dena'ina Athabascan village. After gold was discovered at Resurrection Creek in the 1880s, Tyonek became a major disembarkment point for goods and people. In 1965, the federal court ruled that the Bureau of Indian Affairs had no right to lease Tyonek land for oil development without permission of the Athabascans themselves. The tribe subsequently sold rights to drill for oil and gas beneath the reservation to a group of oil
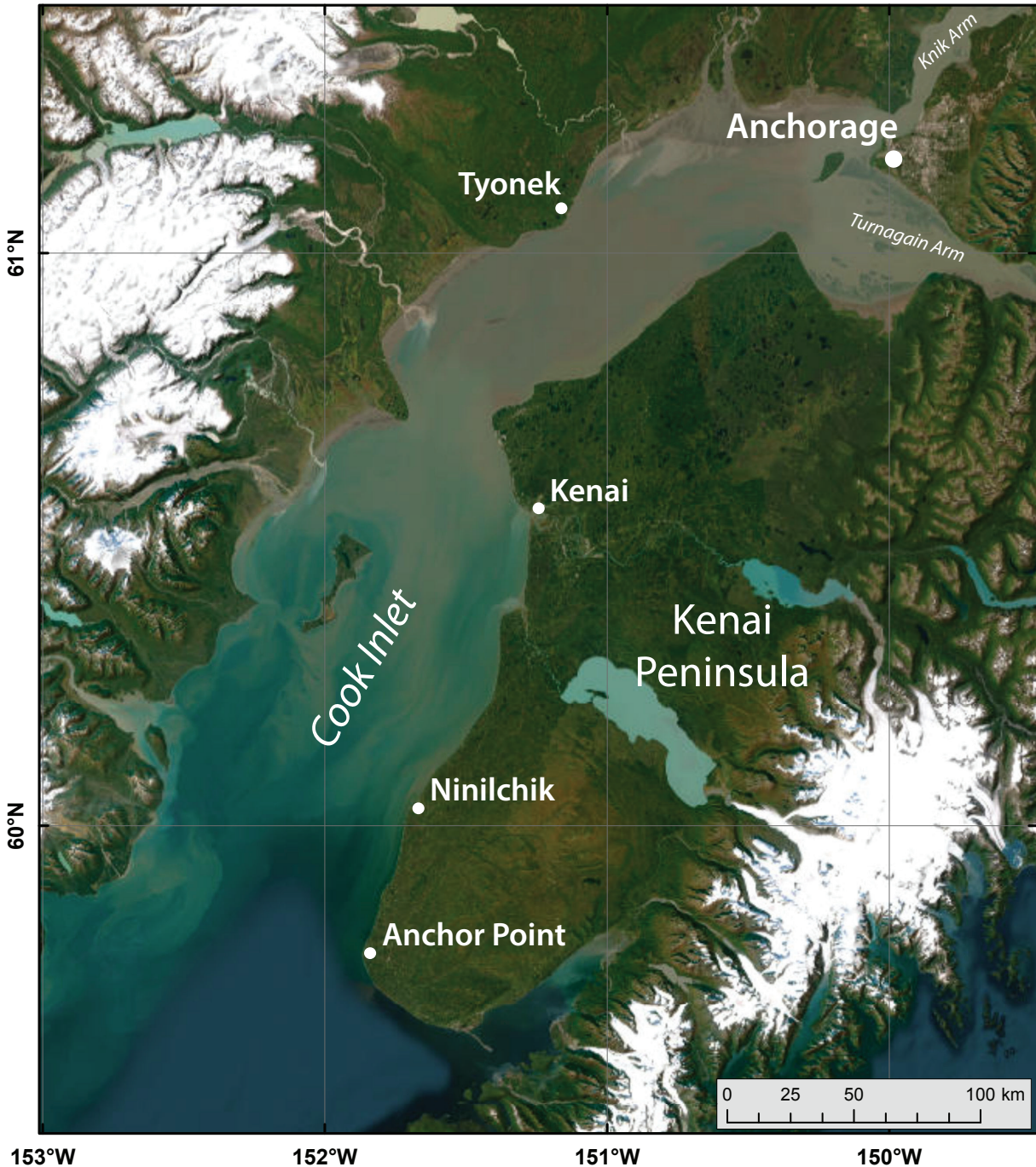
Figure 2. Aerial photograph of Cook Inlet and Kenai Peninsula showing locations of Anchor Point, Kenai, Ninilchik, Tyonek, and Anchorage.

companies for $12.9 million. The reservation status was revoked with the passage of the Alaska Native Claims Settlement Act in 1971. Beluga, a site near Tyonek, is owned by Chugach Electric Association and provides some electricity for Anchorage.

METHODOLOGY AND DATA
Grid Development and Data Sources

We use a series of nested computational grids on the coast of Southcentral Alaska and Cook Inlet to generate detailed maps of potential tsunami inundation triggered by local and distant earthquakes. The coarsest grid, with 2-arc-minute (approximately 2 km [~1.2 mi]) resolution, spans the central and northern Pacific Ocean. We used three intermediate grids between the coarsest- and highest-resolution grids (table 1; fig. 3). The highest-resolution grids (level 4, shaded rectangles in fig. 3) cover coastal waters next to the communities. The spatial resolution of the level 4 grids, with cell dimensions of about 13.2 × 16.4 m (43.3

× 53.8 ft), satisfies National Oceanic and Atmospheric Administration (NOAA) minimum recommended requirements for computation of tsunami inundation (National Tsunami Hazard Mapping Program [NTHMP], 2010).

The map sheets included in this report show the maximum composite extent of inundation for all considered tsunami scenarios and the maximum composite flow depths over dry land. The composite values are calculated as follows: for each tsunami scenario, the tsunami flow depth is computed at each grid point, and at every time step during the tsunami propagation time the maximum value is kept; then we compute the composite maximum flow depth from all considered scenarios by choosing the maximum value for each grid point among all scenarios. The same methodology is used to calculate the composite extent of tsunami inundation. The calculated extent of inundation accounts for coseismic deformation in the communities. Refer to table 2 for maximum uplift and subsidence values associated with each earthquake scenario.

Table 1. Nested grids used to compute propagation of tsunami waves generated in the Pacific Ocean to Cook Inlet communities. The high-resolution grids are used to compute the inundation. Note that the grid resolution in meters is not uniform; the first dimension is the longitudinal grid resolution and the second is the latitudinal resolution.

Grid name	Resolution		West–East boundaries	South–North boundaries
	arc-seconds	feet (meters)		
Level 0, Northern Pacific	120 × 120	≈9,629 x 12,139 (2,935 × 3,700)	120°00' E–60°00' W	60°00' S–65°00' N
Level 1, Southcentral Alaska	24 × 24	≈ 1,269 x 2,428 (387 × 740)	156°00' W–145°00' W	55°00' N–62°00' N
Level 2, Cook Inlet	8 × 8	≈ 404 x 810 (123 × 247)	154°30' W–148°50' W	58°30' N–61°42' N
Level 3, Fine resolution, upper Cook Inlet	8/3 × 8/3	≈ 131 x 269 (40 × 82)	152°36' W–148°54' W	60°15' N–61°40' N
Level 4, High resolution, Anchor Point	8/9 × 1/2	≈ 43 × 52 (13 x 16)	151°58'59" W–151°47'37" W	59°40'55" N–59°51'54" N
Level 4, High resolution, Kenai	8/9 × 1/2	≈ 43 × 52 (13 x 16)	151°28'18" W–151°04'05" W	60°16'47" N–60°49'13" N
Level 4, High resolution, Ninilchik	8/9 × 1/2	≈ 43 × 52 (13 x 16)	151°45'51" W–151°36'37" W	60°00'45" N–60°06'12" N
Level 4, High resolution, Tyonek	8/9 × 1/2	≈ 43 × 52 (13 x 16)	151°12'57" W–150°59'41" W	61°01'07" N–61°12'08" N
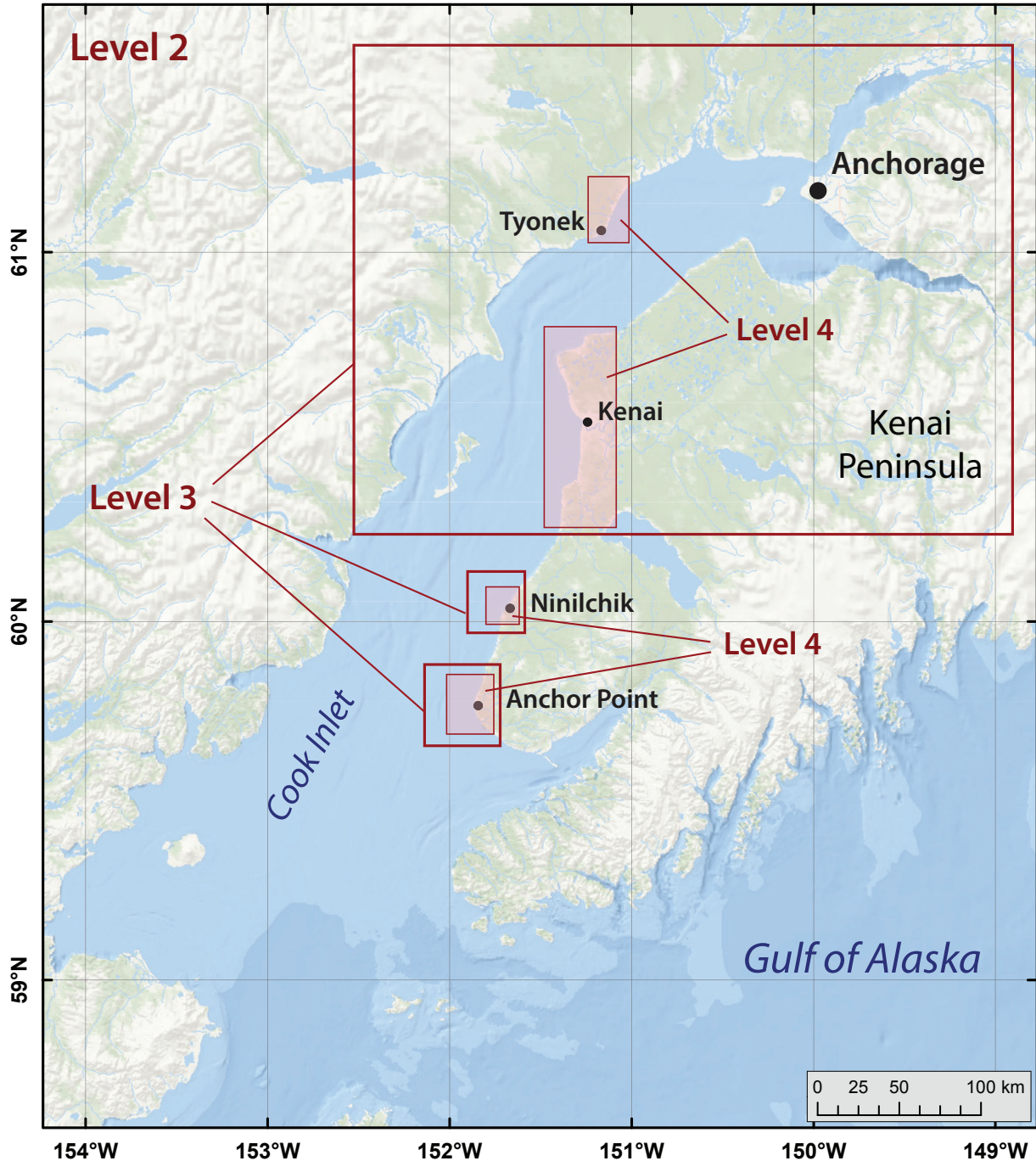
Figure 3. Nesting of the levels 2–4 bathymetry/topography grids for numerical modeling of tsunami propagation and runup in Cook Inlet. Each embedded grid is outlined by a red rectangle. The shaded rectangles are the high-resolution level 4 grids.

Numerical Model of Tsunami Propagation and Runup

To estimate tsunami propagation and runup in Cook Inlet we used the same numerical modeling techniques as previous Alaska tsunami inundation studies (for example, Suleimani and others, 2010, 2013, 2015, 2016; Nicolsky and others, 2011a, 2013, 2014, 2015). All hypothetical tsunami simulations were conducted using the bathymetric/topographic data corresponding to the Mean Higher High Water (MHHW) tide level in Cook Inlet. We use a conservative approach and

assume that all simulated tsunamis arrive during high tides and with consideration to tectonic land-level changes (i.e., subsidence or uplift) caused by hypothetical earthquakes.

The numerical modeling results presented in this report are relevant for existing sea level conditions and do not account for changes in water levels caused by global sea level rise, regional tectonic processes, and isostatic rebound. Even though the report on global sea level changes for 2050 and 2100 by the Intergovernmental Panel on Climate Change (Oppenheimer and others, 2019) predicts global sea level rise, rapid regional uplift in southern Alaska caused by ice loss contributes to negative sea level changes in the region (Larsen and others, 2004; Shirzaei and others, 2021).

TSUNAMI SOURCES

Great historical earthquakes along the Alaska–Aleutian subduction zone occurred on the mega-thrust—the fault, or contact surface, between the subducting Pacific plate and the overriding North American plate (fig. 1). Friction between the two converging plates keeps them stuck, or "locked" together at the edges. Relative plate motion causes energy to accumulate at the plate boundaries and this energy is eventually released during sudden slip in an earthquake. It is theorized that the strain energy primarily accumulates in the locked, or coupled, patches of the megathrust where friction on the fault is greatest. Our goal is to evaluate the tsunami effects resulting from all plausible combinations of slip patches that may rupture in the next great earthquake.

The detailed description of the earthquake history and tectonic regime at the eastern end of the Alaska–Aleutian subduction zone (fig. 1) is given in the "Tectonic Setting" section of the upper Cook Inlet tsunami mapping study by Suleimani and others (2023). In the same publication, the "Modeling of the 1964 Tsunami in Cook Inlet" section provides analysis of complex tsunami–tide interactions in Cook Inlet and explains the reason for the unreported tsunami and lack of damage in

Anchorage during the 1964 Great Alaska Earthquake. Using a dynamically coupled model of tsunami and tides for Cook Inlet, we demonstrated that static-tide numerical model runs with the MHHW vertical datum do not underestimate tsunami effects in Cook Inlet and result in a conservative estimate of the inundation zone.

To perform a comprehensive tsunami hazard assessment for Cook Inlet communities, we consider variable slip distributions on neighboring segments of the interface—both along strike as well as at different depths. First, we conduct a sensitivity study to determine what effect the down-dip location of a rupture has on tectonic subsidence, uplift, and resulting tsunami waves. We then apply the results of the sensitivity study to construct the maximum credible scenarios.

Sensitivity Study

Earthquake ruptures with slip at different depths have different wave-generating potential, result in different distributions and amounts of subsidence and uplift in coastal communities, and therefore result in different tsunami and permanent flooding characteristics. The point of the sensitivity study is to determine the most dangerous down-dip location on the megathrust for a hypothetical earthquake to occur. We use the USGS SLAB2 model of the Alaska–Aleutian plate interface developed by Hayes (2018; fig. 4). Like the plate interface model used by Zweck and others (2002), the SLAB2 plate interface exhibits a relatively shallow dip beneath Prince William Sound (PWS) and Kenai Peninsula (KP) until it reaches a depth of 30 km (18.6 mi), at which point it steepens (fig. 4). This deep area also corresponds to the unlocked or weakly coupled part of the plate interface (Zweck and others, 2002).

The plate interface is discretized into a mesh of rectangles ranging from 1 to 6 km (0.6 to 3.7 mi) in the along-strike direction of the plate interface, with denser discretization in its shallow, or uppermost part (fig. 4). The upper and lower edges of each rectangle coincide with depth contours of the plate interface that are spaced at
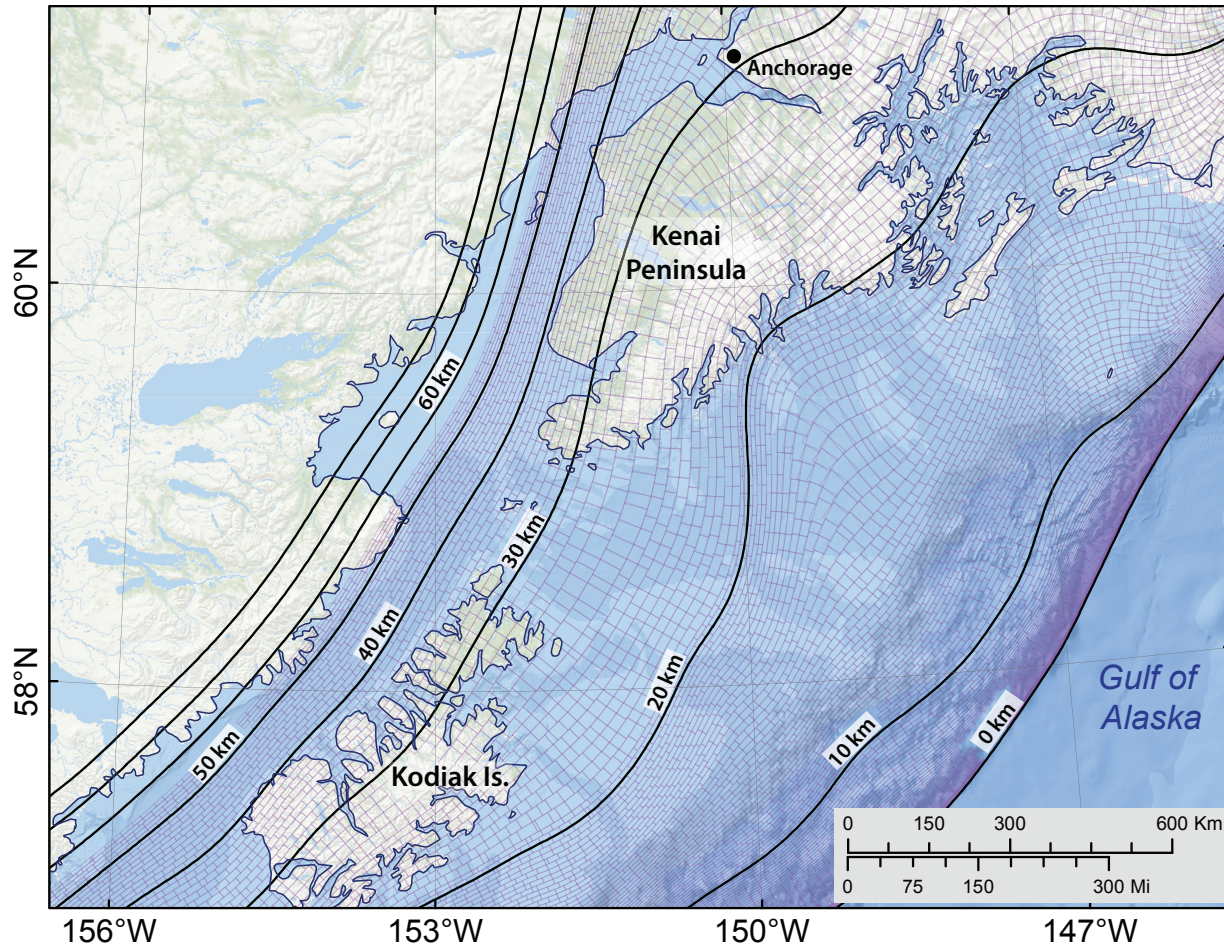
Figure 4. Discretization of the plate interface used to compute the coseismic vertical displacements with formulae developed by Okada (1985). Black lines mark depth contours (in kilometers) of the plate interface and the purple rectangles represent individual pieces of the plate considered by the model.

0.5 km (0.3 mi), with spacing of 0.25 km (0.16 mi) at the shallowest part of the plate interface. The rectangles, called subfaults, are later used to compute coseismic ground deformation (Okada, 1985). Using this discretization of the plate interface, we model potential earthquake scenarios by prescribing a general pattern of slip distribution in the proposed rupture, then computing the slip at the center of each subfault using seismic moment (i.e., earthquake magnitude) as a constraint.

We develop four different slip cases (cases A–D) for M_w 8.0 earthquakes and calculate vertical seafloor deformations associated with each case (fig. 5). The slip distribution for all four cases is uniform in the along-strike direction with tapering at the ends of the rupture. The assumed slip distribution is consistent with earthquake source scenarios used by other tsunami modeling studies (for example, Butler, 2014; USGS SAFRR scenario, www.usgs.gov/centers/western-geographic-science-center/science/safrr-tsunami-scenario). Between any two consecutive cases, the hypothetical rupture is offset by about 10 km (6.2 mi) in the downdip direction: case A corresponds to a shallow surface-breaching rupture with maximum slip located close to the trench; cases B, C, and D correspond to ruptures with maximum slip roughly centered at depth of 10 km (6.2 mi), 20 km (12.4 mi), and 30 km (18.6 mi), respectively.

Simulated water levels in lower Cook Inlet communities vary considerably according to different slip distributions (fig. 6). The time series indicate that the ruptures at 30 km (18.6 mi) depth

(case D) result in the highest wave amplitude in all locations, followed by cases C, the rupture at a depth of 20 km (12.4 mi), and B, the rupture at a depth of 10 km (6.2 mi). The shallow surface-breaching rupture represented by case A produces the smallest waves. Based on these results, we develop hypothetical ruptures with maximum slip in the 20–40 km (12.4–24.8 mi) depth range (cases C–D). As in Nicolsky and others (2016), we develop maximum credible scenarios by allowing up to 35 m (115 ft) of slip in the deep and intermediate sections of the Alaska–Aleutian megathrust and up to 50 m (164 ft) in the shallow sections of the megathrust. The maximum slip is imposed along regions of the

megathrust that have the capability to generate the highest amplitude waves in Cook Inlet.

Hypothetical Tsunami Sources

In this section, we describe tsunamigenic Alaska–Aleutian megathrust earthquakes used for assessing tsunami hazard in Cook Inlet (table 2). Our goal is to determine geologically plausible scenarios that will result in maximum reasonable tsunami inundation, that is: credible worst-case scenarios. Scenarios are grouped according to their locations and specific source characterization. Group I includes M_W 9.2 tsunami sources in Kenai Peninsula (KP) and Kodiak Island (KI) segments
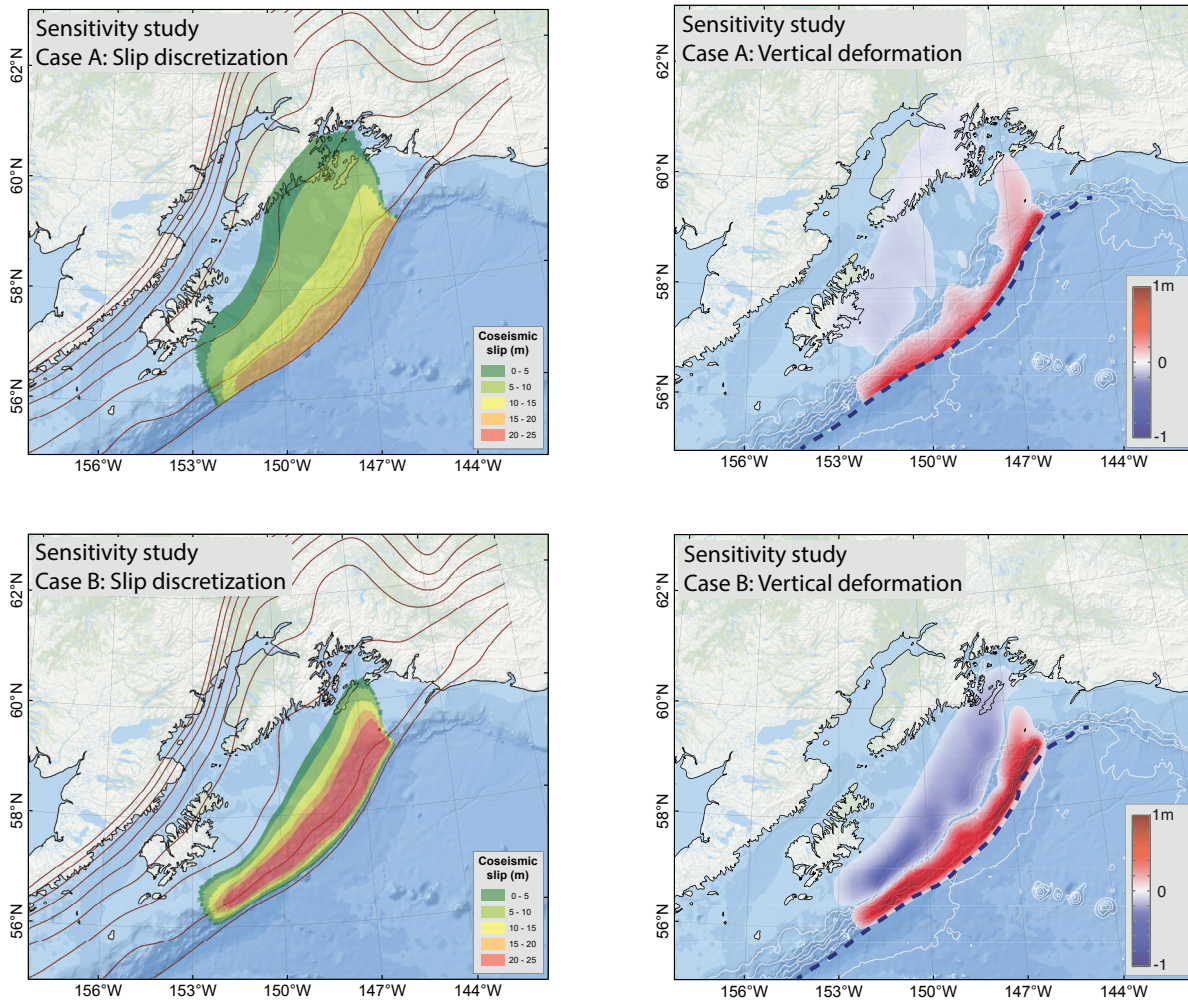
Figure 5. Imposed slip distributions along the plate interface (left) and computed vertical ground surface deformation (right) for sensitivity cases A and B, modeling M_W 8.0 ruptures near the Kenai Peninsula. The slip location varies in the downdip direction of the plate interface while preserving the same slip patch configuration. Red lines in the left images are depth contours of the subduction interface from 0-80 km with a 10-km interval. White lines in the right images are bathymetry contours within the depth range 1–5 km with a 1-km interval and the dashed blue line is the location of the seafloor trench.

Figure 5, continued. Imposed slip distributions along the plate interface (left) and computed vertical ground surface deformation (right) for sensitivity cases C and D, modeling M_W 8.0 ruptures near the Kenai Peninsula. The slip location varies in the downdip direction of the plate interface while preserving the same slip patch configuration. Red lines in the left images are depth contours of the subduction interface from 0-80 km with a 10-km interval. White lines in the right images are bathymetry contours within the depth range 1–5 km with a 1-km interval and the dashed blue line is the location of the seafloor trench.

with predominantly shallow slip. Group II includes scenarios that are based on results of the sensitivity study. Scenarios in Group III represent potential tsunami sources with magnitudes M_W 8.8 and M_W 8.9 with the maximum slip located at different depths of the plate interface in the area between KP and KI. Group IV includes scenarios in the KI and Alaska Peninsula (AP) segments, which model tsunamis propagating into Cook Inlet through Shelikof Strait (fig. 1), including the USGS SAFRR scenario (Ross and Jones, 2013). We build scenarios in Group V considering implications of the 2011 Tohoku earthquake (Wang and others,

2018), which assume that the maximum slip near the trench could be up to 50 m (164 ft). To be consistent with previous reports (e.g., Nicolsky and others, 2016, 2017; Suleimani and others, 2016), we consider scenarios with slip parameterization like that proposed by Butler and others (2014). Finally, Group VI consists of a single scenario, which models a rupture of the Cascadia subduction zone as an example of a distant tsunami source.

In all scenarios, we do not account for the finite speed of rupture propagation along the fault, and we consider the ocean-bottom displacements to be instantaneous. All proposed scenarios are

summarized in table 2. The proposed slip distributions and vertical coseismic deformations are shown in figure 7. We consider various downdip locations for the maximum slip to parameterize various credible tsunamigenic earthquakes. In the downdip direction, the slip is determined by the slip skewness parameter q in the Freund and Barnett (1976) formulae. For each scenario, the maximum slip is assumed to be located at a different depth range. We note that the presented scenarios are intended to capture the maximum credible scenarios and to provide a starting point for development of more complex models.

A

B
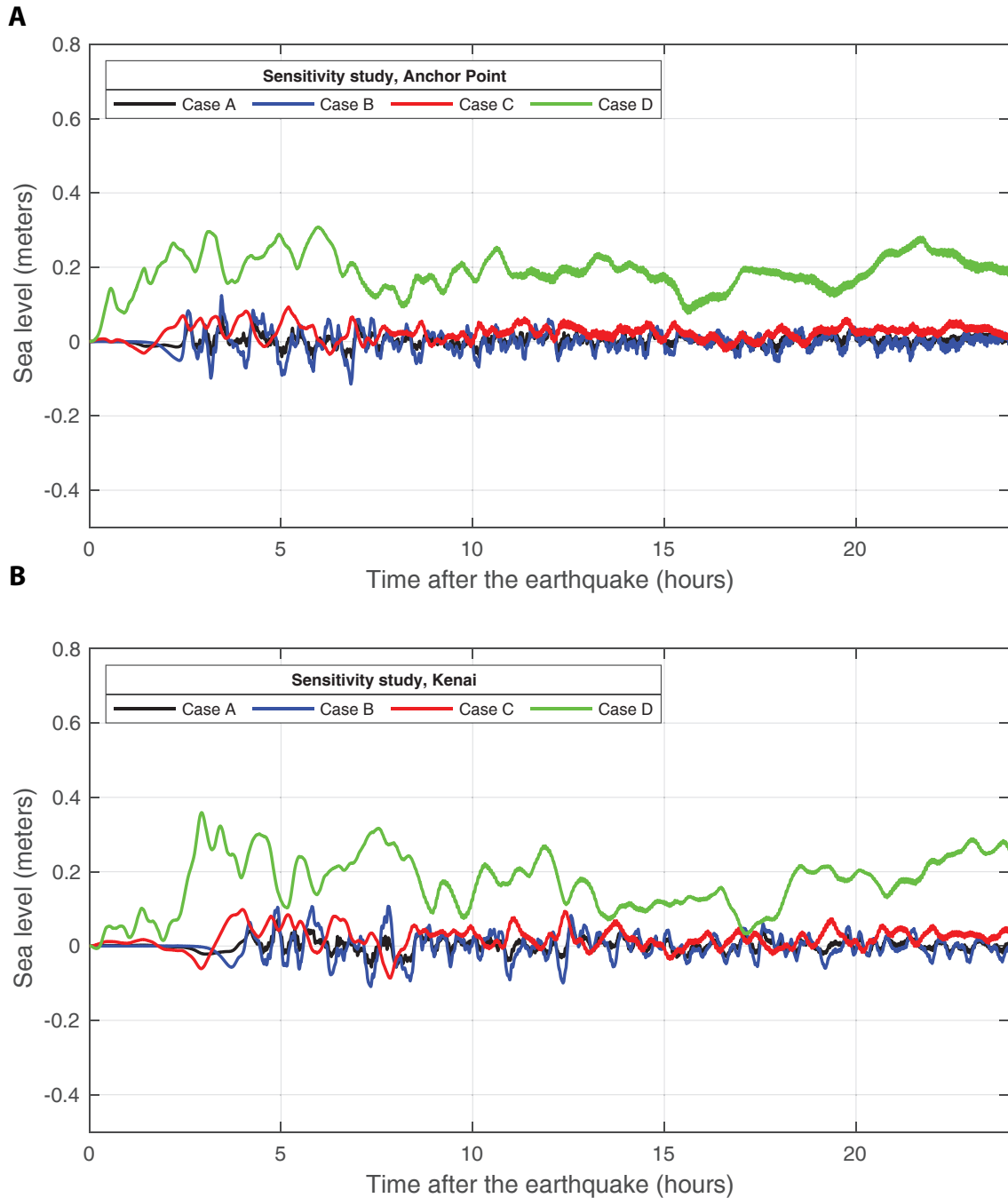
Figure 6. Modeled water-level dynamics (from the point of view of an observer standing at the shore) at (**A**) Anchor Point and (**B**) Kenai for the ground surface deformations shown in figure 5. Model duration is 24 hours. The zero value of sea level corresponds to the post-earthquake MHHW level. The increasing thickness of the green line reflects small-magnitude, high-frequency fluctuations in the model output.

C

D
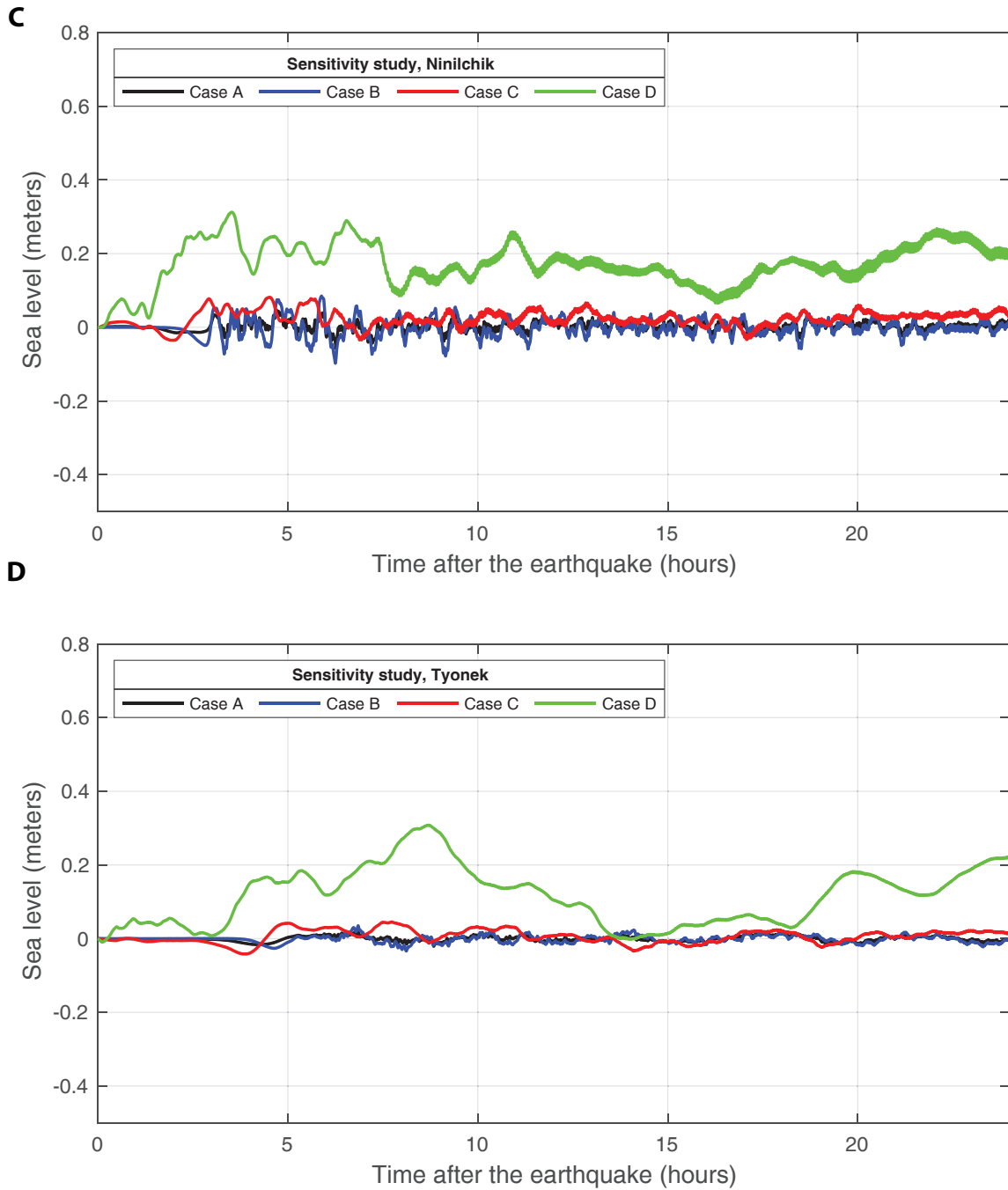
Figure 6, continued. Modeled water-level dynamics (from the point of view of an observer standing at the shore) at (**C**) Ninilchik and (**D**) Tyonek for the ground surface deformations shown in figure 5. Model duration is 24 hours. The zero value of sea level corresponds to the post-earthquake MHHW level. The increasing thickness of the green line reflects small-magnitude, high-frequency fluctuations in the model output.

Table 2. The hypothetical megathrust scenarios in the Gulf of Alaska (except for scenario 16), used to model tsunami runup in Cook Inlet communities. Asterisk indicates scenarios that have been considered in previous inundation mapping reports.

Group	#	M_W	Description	Depth range km (mi)	Maximum slip depth range km (mi)	Maximum slip m (ft)	Maximum subsidence m (ft)	Maximum uplift m (ft)
I	1*	9.2	Earthquake in the KI-KP region: Predominantly shallow slip with maximum slip at a depth of 10-15 km	0–25 (0–15.5)	10–15 (6.2–9.3)	51.6 (169.2)	7.3 (23.9)	10.7 (35.1)
	2*	9.2	Earthquake in the KI-KP region: Predominantly shallow slip with maximum slip at a depth of 0-10 km	0–25 (0–15.5)	0–10 (0–6.2)	48.3 (158.5)	5.4 (17.7)	14.2 (46.6)
II	3*	9.1	Earthquake in the PWS-KP-KI region: maximum slip at a depth of 18–32 km	15–50 (9.3–31.0)	18–32 (11.2–19.9)	37.2 (122.0)	7.5 (24.6)	8.9 (29.1)
	4*	9.1	Earthquake in the PWS-KP-KI region: maximum slip at a depth of 25–35 km	15–50 (9.3–31.0)	25–35 (15.5–21.7)	37.0 (121.4)	6.5 (21.3)	7.0 (23.0)
	5*	9.0	Earthquake in the PWS-KP-KI region: maximum slip at a depth of 28–42 km	15–50 (9.3–31.0)	28–42 (17.4–26.0)	37.0 (121.4)	4.7 (15.4)	7.1 (23.3)
	6*	9.2	Earthquake in the PWS-KP-KI region: maximum slip at a depth of 17–32 km	12–50 (7.4–31.0)	17–32 (10.6–19.9)	35.4 (116.1)	7.3 (23.9)	7.1 (23.3)
	7*	9.1	Earthquake in the PWS-KP-KI region: maximum slip at a depth of 20–40 km	17–50 (10.5–31.0)	20–40 (12.4–24.8)	37.1 (121.7)	5.7 (18.7)	7.0 (23.0)
	8	9.1	Earthquake in the PWS-KP-KI region: maximum slip at a depth of 17-42 km	12–50 (7.4–31.0)	17–42 (10.5–26.1)	35 (21.7)	5.1 (16.7)	6.8 (22.3)
III	9	8.8	Earthquake in the PWS-KP-KI region: maximum slip at a depth of 32-38 km	15–40 (9.3–24.8)	32-38 (19.9–23.6)	35 (21.7)	3.5 (11.5)	5.5 (18.0)
	10	8.9	Earthquake in the PWS-KP-KI region: maximum slip at a depth of 27-32 km	17–40 (10.5–24.8)	27-32 (16.8–19.9)	35 (21.7)	6.2 (20.3)	5.6 (18.3)
IV	11*	8.9	Earthquake in the KI-AP region: maximum slip at a depth of 15–25 km	10–30 (6.2–18.6)	15–25 (9.3–15.5)	36.9 (121.0)	6.9 (22.6)	9.9 (32.4)
	12*	8.8	Earthquake in the KI-AP region: maximum slip at a depth of 25–35 km	20–40 (12.4–24.8)	25–35 (15.5–21.7)	37.0 (121.4)	5.4 (17.7)	9.2 (30.2)
	13*	9.0	SAFRR scenario (Ross and others, 2013)	0–50 (0–31.0)	5–20 (3.1–12.4)	65.0 (213.2)	2.8 (9.2)	14.8 (48.6)
V	14*	9.3	Earthquake in the PWS-KP-KI region: 50 m of maximum slip close to the trench	2–38 (1.2–23.6)	5–12 (3.1–7.4)	50 (164.0)	2.7 (8.8)	20.0 (65.6)
	15*	9.3	Earthquake in the PWS-KP-KI region: 35 m of maximum slip across the majority of the rupture	2–38 (1.2–23.6)	5–22 (3.1–13.7)	35.0 (115.0)	8.0 (26.2)	13.7 (44.9)
VI	16*	9.1	Earthquake in the Cascadia subduction zone (Wang and others, 2003)	?	?	45.0 (148.0)	8.0 (25.0)	11.0 (35.0)
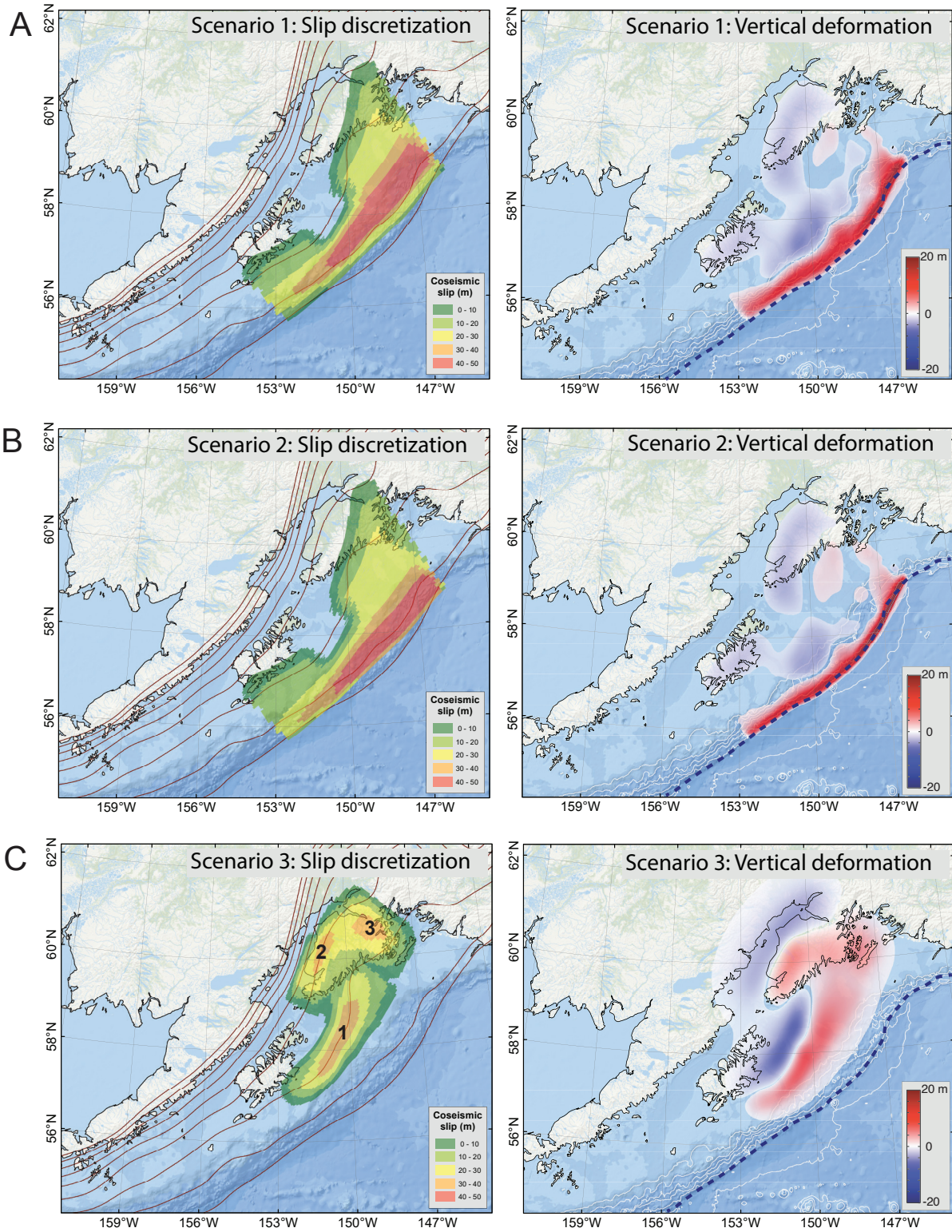
Figure 7A–C. Estimated slip distribution along the plate interface for scenarios 1–3 and computed vertical ground surface deformation for scenarios 1–3. Red lines are depth contours of the subduction interface within the depth range 0–80 km with a 10-km interval. White lines are bathymetry contours within the depth range 1–5 km with a 1-km interval, and dashed blue line is the location of the seafloor trench.
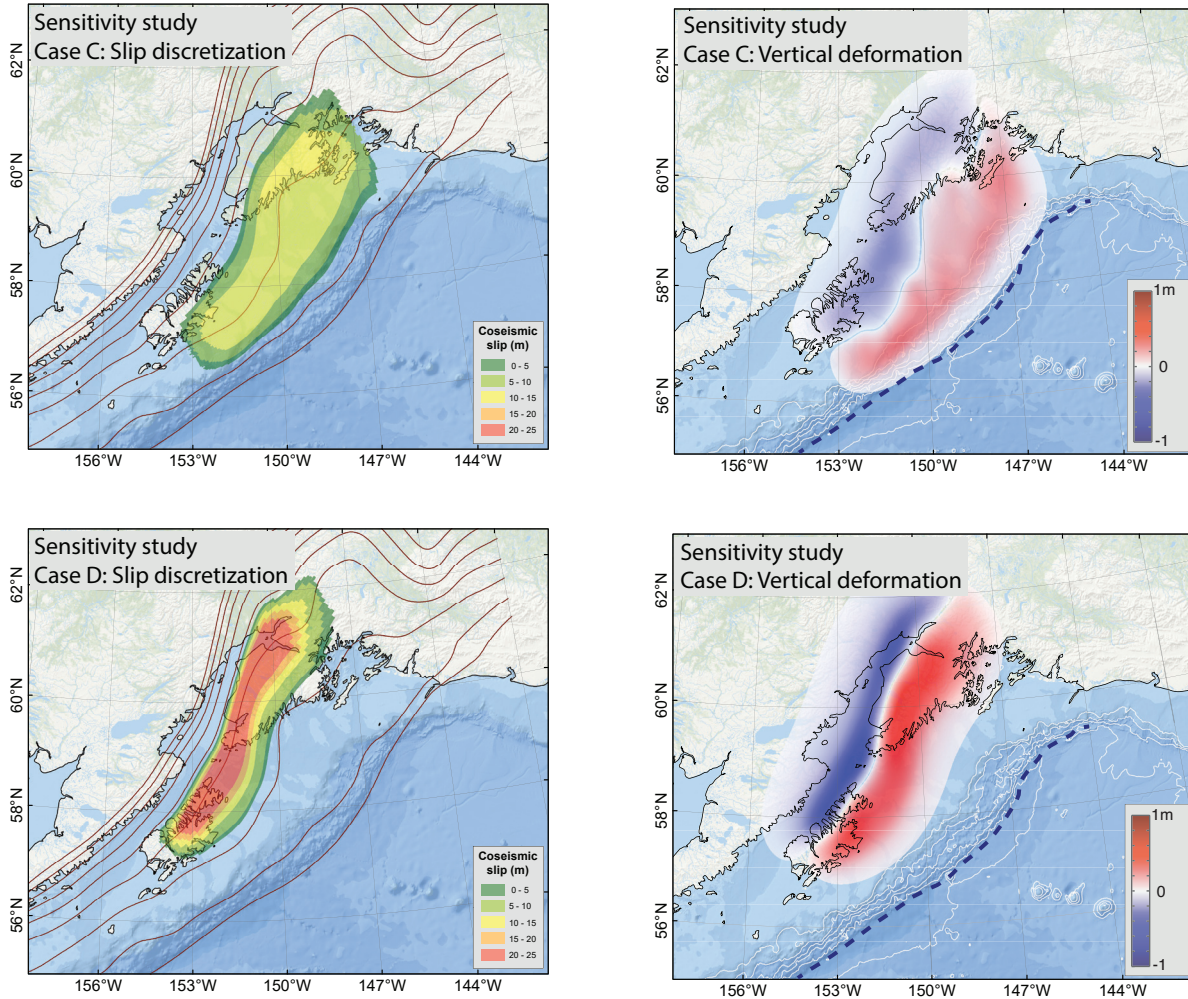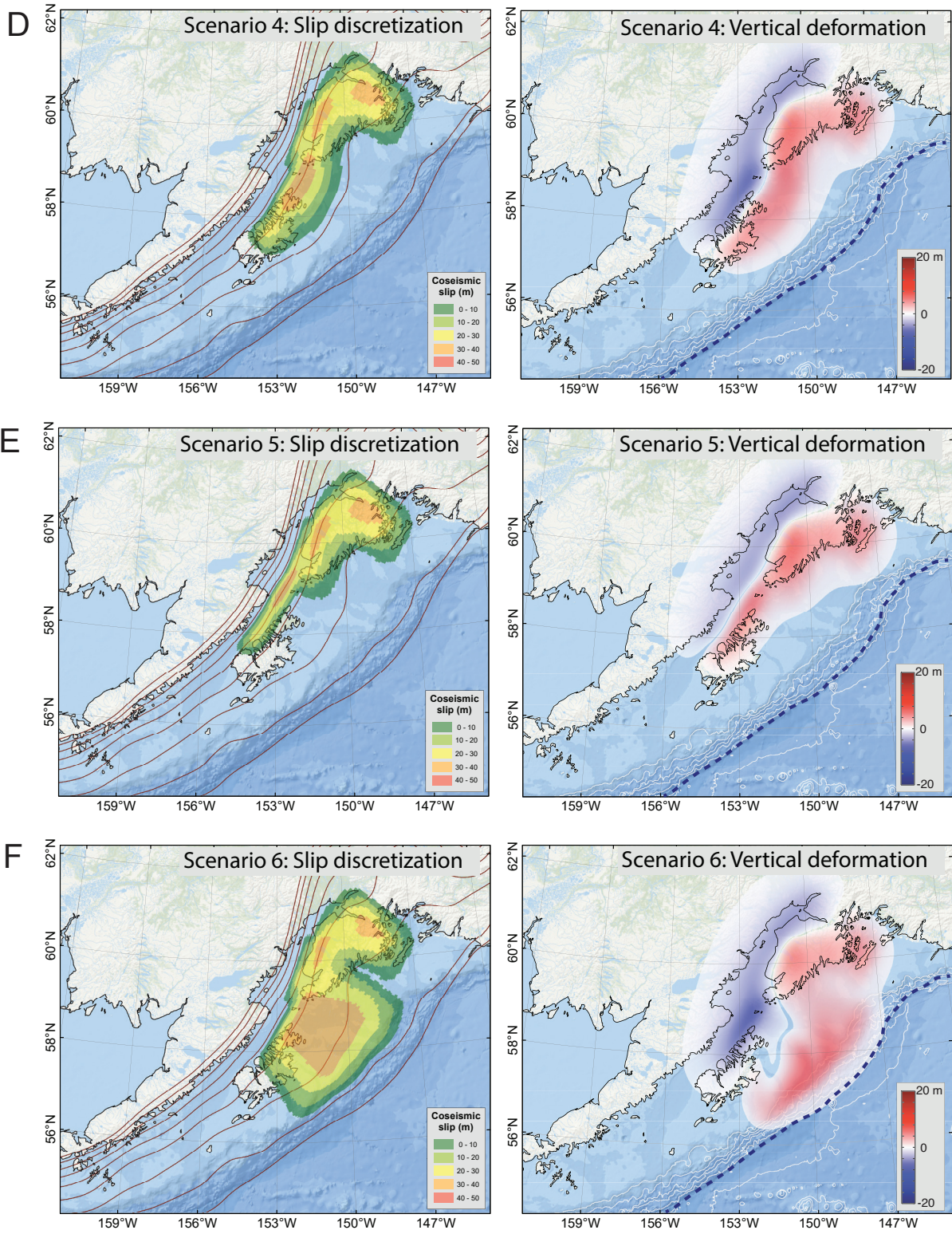
Figure 7D–F. Estimated slip distribution along the plate interface for scenarios 4–6 and computed vertical ground surface deformation for scenarios 4–6. Red lines are depth contours of the subduction interface within the depth range 0–80 km with a 10-km interval. White lines are bathymetry contours within the depth range 1–5 km with a 1-km interval, and dashed blue line is the location of the seafloor trench.
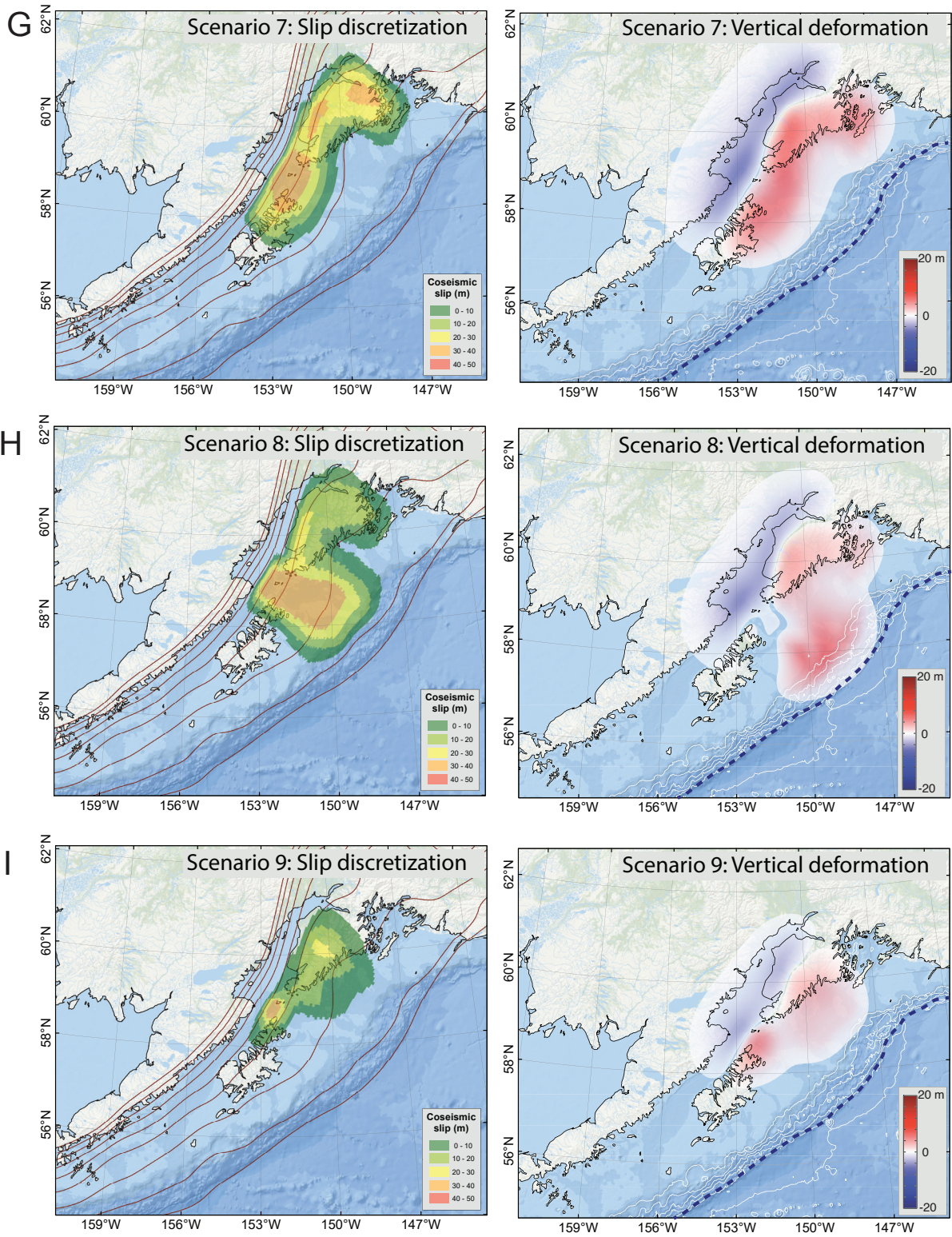
Figure 7G–I. Estimated slip distribution along the plate interface for scenarios 7–9 and computed vertical ground surface deformation for scenarios 7–9. Red lines are depth contours of the subduction interface within the depth range 0–80 km with a 10-km interval. White lines are bathymetry contours within the depth range 1–5 km with a 1-km interval, and dashed blue line is the location of the seafloor trench.
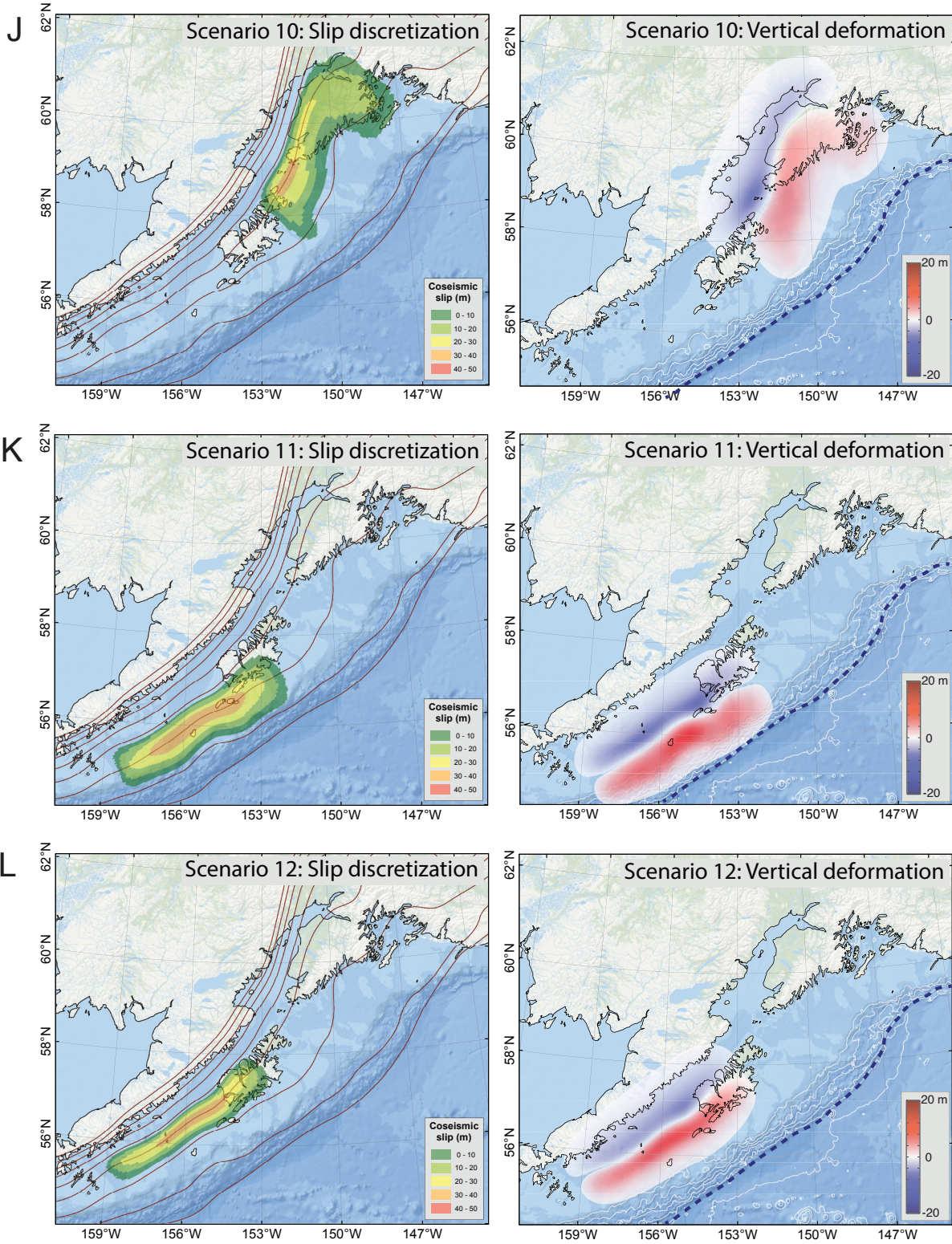
Figure 7J–L. Estimated slip distribution along the plate interface for scenarios 10–12 and computed vertical ground surface deformation for scenarios 10–12. Red lines are depth contours of the subduction interface within the depth range 0–80 km with a 10-km interval. White lines are bathymetry contours within the depth range 1–5 km with a 1-km interval, and dashed blue line is the location of the seafloor trench.
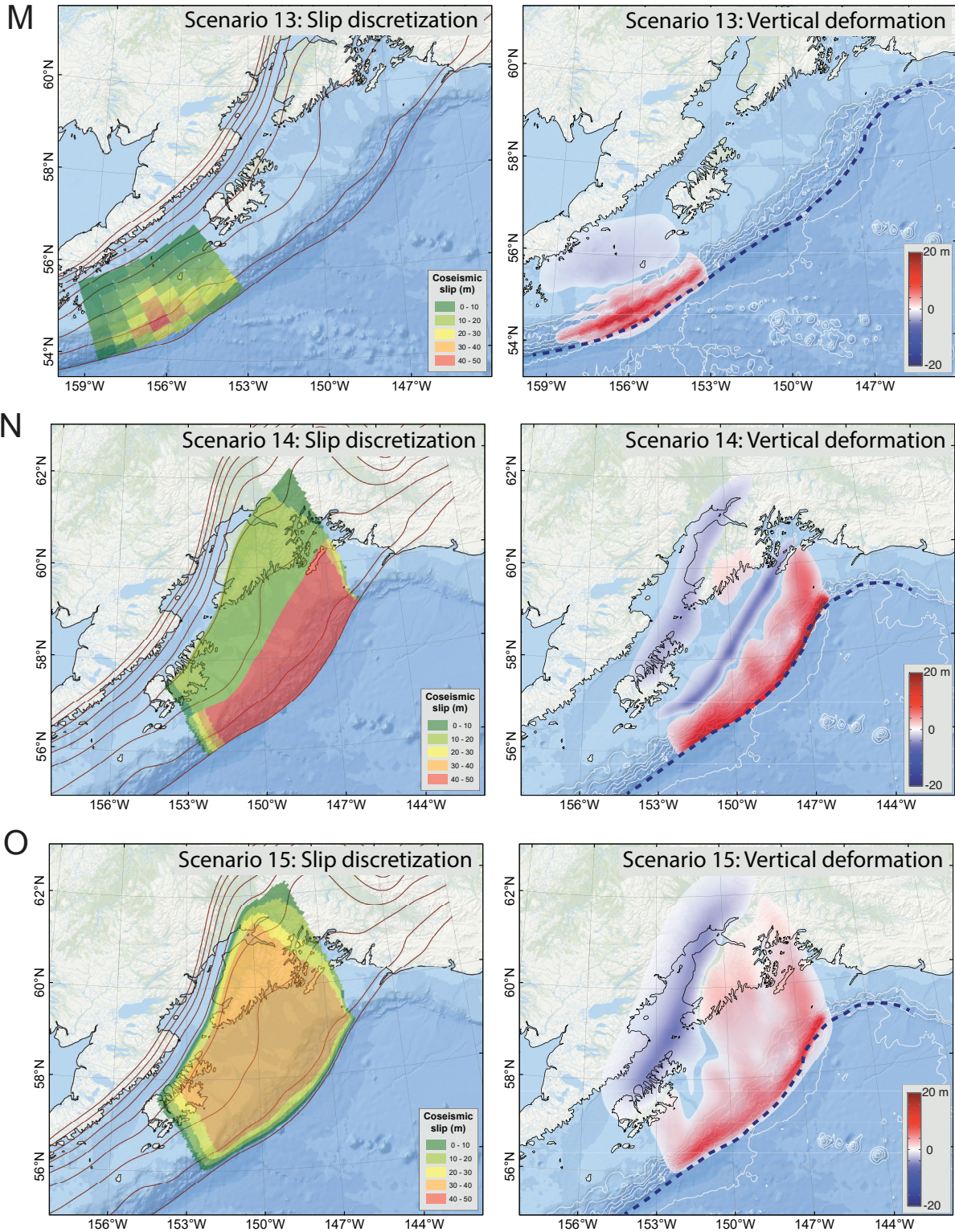
Figure 7M–O. Estimated slip distribution along the plate interface for scenarios 13–15 and computed vertical ground surface deformation for scenarios 13–15. Red lines are depth contours of the subduction interface within the depth range 0–80 km with a 10-km interval. White lines are bathymetry contours within the depth range 1–5 km with a 1-km interval, and dashed blue line is the location of the seafloor trench.

P
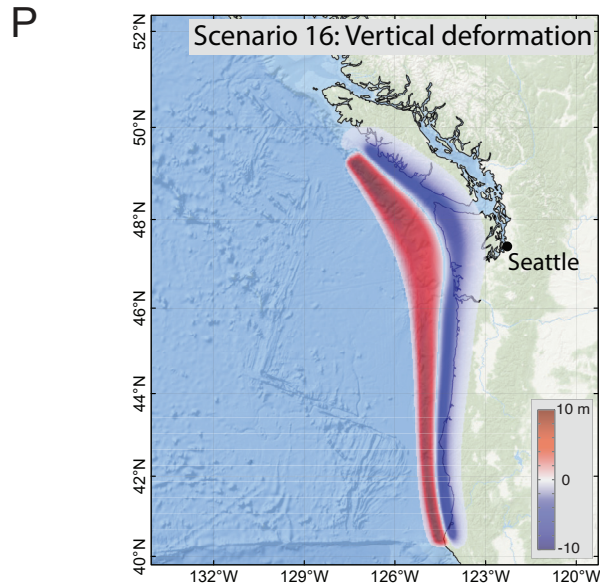
Figure 7P. Computed vertical ground surface deformation for scenario 16 (slip distribution is not provided this scenario).

Group I

These scenarios were used in the Homer tsunami inundation modeling study (Suleimani and others, 2019). They incorporate inferences made from modern geodetic data about the coupling between the Pacific and North American plates—that certain down-dip regions of the plate interface between KP and KI are steadily slipping during the interseismic period and are not accumulating elastic strain energy at the same rate as the rest of the plate interface. Therefore, we do not assign slip to these regions but propose that a hypothetical rupture might propagate to shallow depths and produce a large amount of slip close to the trench. The proposed slip distributions and vertical coseismic deformations for scenarios 1–2 are shown in figure 7A–B.

Scenario 1: M$_W$ 9.2 earthquake in the KI-KP region: Predominantly shallow slip with maximum slip at a depth of 10–15 km (6.2–9.3 mi).	The source consists of KI and PWS asperities, separated by the gap and connected by the slip in the shallow part of the rupture. The maximum slip of 51.6 m (169.2 ft) is at a depth of 10–15 km (6.2–9.3 mi). Maximum slip is at the eastern end of the shallow part of the rupture decreasing toward its western end.
Scenario 2: M$_W$ 9.2 earthquake in the KI-KP region: Predominantly shallow slip with maximum slip at a depth of 0–10 km (0–6.2 mi).	The source consists of KI and PWS asperities, separated by the gap and connected by the slip in the shallow part of the rupture. The maximum slip of 48.3 m (158.5 ft) is at a depth of 0–10 km (0–6.2 mi). Maximum slip is at the eastern end of the shallow part of the rupture decreasing toward its western end.

Group II

Scenarios in this group are based on the results of the sensitivity study, with additional constraints derived from paleoseismic studies in KP. Shennan and others (2008) present geologic evidence of six prehistoric tsunamigenic earthquakes in the KP area of Southcentral Alaska in the past 4,000 years based on radiocarbon ages of tidal marsh deposits in Girdwood (fig. 2). The Girdwood marsh provides the most comprehensive record of Holocene great earthquakes in Southcentral Alaska. All seven great earthquakes, including the 1964 event, resulted in similar amounts of subsidence in Girdwood. However, despite there being an excellent record of subsidence during great earthquakes at Girdwood, there is no recorded evidence of tsunami inundation. There is no clear correlation between the amount of subsidence and the time since the previous great earthquake, although the smallest amount of subsidence occurred after the shortest preceding interval (Shennan and others, 2008).

We also employ results of the Kenai Peninsula paleoseismic study by Kelsey and others (2015) by assuming that the KP segment can rupture in a future event. Therefore, we create scenarios that have the maximum amount of slip placed at different depths of the plate interface in the KP segment, at the same time ensuring that Girdwood remains in the region of subsidence for each coseismic deformation pattern. Another goal was to create scenarios that generate an N-wave entering Cook Inlet—meaning that the wave trough travels first, followed by the wave crest. This is achieved by arranging slip patterns in such a way that the resulting coseismic deformation causes subsidence in Cook Inlet. The proposed slip distributions and vertical coseismic deformations for scenarios 3–8 are shown in figure 7C–H. In each rupture, there are three patches of high slip: in the area between KP and KI (patch 1 in fig. 7C), at the western end of KP (patch 2), and at the eastern part of KP west of PWS (patch 3). The location of patches 2 and 3 are the same for all ruptures, but the down-dip location of patch 1 varies according to the results of the sensitivity study.

Scenario 3: M_W 9.1 earthquake in the PWS-KP-KI region: maximum slip at a depth of 18–32 km (11.2–19.9 mi).	The depth of patch 1 corresponds to the depth for sensitivity case C: patch 1 is centered around the depth of 20 km (12.4 mi).
Scenario 4: M_W 9.1 earthquake in the PWS-KP-KI region: maximum slip at a depth of 25–35 km (15.5–21.7 mi).	The depth of patch 1 corresponds to the depth for sensitivity case D: patch 1 is centered around the depth of 30 km (18.6 mi).
Scenario 5: M_W 9.0 earthquake in the PWS-KP-KI region: maximum slip at a depth of 28–42 km (17.4–26.0 mi).	Patch 1 of higher slip is centered around the depth of 40 km (24.8 mi). This is the deepest location of the high slip in that area among all ruptures.

Scenario 6: M$_W$ 9.2 earthquake in the PWS-KP-KI region: maximum slip at a depth of 17–32 km (10.6–19.9 mi).	The depth of patch 1 corresponds to that of the combination of sensitivity cases C and D: patch 1 is spread in the depth region between approximately 20 and 30 km.
Scenario 7: M$_W$ 9.1 earthquake in the PWS-KP-KI region: maximum slip at a depth of 20–40 km (12.4–24.8 mi).	The depth of maximum slip corresponds to that of the combination of sensitivity case D and a deeper rupture at 40 km (24.8 mi): patch 1 is spread in the depth region between approximately 30 and 40 km.
Scenario 8: M$_W$ 9.1 earthquake in the PWS-KP-KI region: maximum slip at a depth of 17-42 km (10.6–26.1 mi).	The depth of maximum slip corresponds to that of the combination of sensitivity cases C, D, and a deeper rupture at 40 km (24.8 mi): patch 1 is spread in the depth region between approximately 20 and 40 km.

Group III

Scenarios in this group represent potential large earthquakes with magnitudes M$_W$ 8.8 and M$_W$ 8.9, and with maximum slip located at different depths of the plate interface in the area between KP and KI. These scenarios allow for future ruptures with slip distribution that differ from what was observed in 1964 and in locations that may not align with current deformation observations. We base these scenarios on the Kenai Peninsula paleoseismic study (Kelsey and others, 2015) concluding that the KP segment, which is presently creeping, can rupture independently of the adjacent PWS segment, which is presently locked. The objective here is not to limit our assessment of future tsunami hazards by using only historically observed slip patterns and geodetic models. For the scenarios in this group, we allow the maximum slip of 37 m (121.4 ft) at different depths

of the plate interface in hypothetical ruptures and assume that the 1964 earthquake had no effect on the current degree of plate locking or accumulated slip deficit in the KP segment. This approach allows us to determine whether the inclusion of slip in the KP segment in deformation models will result in run-up values in Cook Inlet communities comparable to that from source models that are constrained by geodetic and geologic data. At the same time, we are assessing the tsunami impact from earthquakes of lower magnitudes that have potentially shorter recurrence intervals. The average and maximum slip as well as the rupture areas for scenarios 9 and 10 are set according to the scaling relations of Papazachos and others (2005) and Moss and Travasarou (2006). The proposed slip distributions and vertical coseismic deformations for scenarios 9 and 10 are shown in figure 7I and J.

Scenario 9: M$_W$ 8.8 earthquake in the KP region: maximum slip at a depth of 32–38 km (19.9–23.6 mi).	This is a deep rupture with the region of maximum slip of 37 m (121.4 ft) centered around the depth of 40 km (24.8 mi) in the area between KP and KI.

Scenario 10: M$_W$ 8.9 earthquake in the KP region: maximum slip at a depth of 28–42 km (17.4–26.0 mi).	This is a deep rupture, similar to scenario 9, but with the region of maximum slip of 37 m (121.4 ft) centered around the depth of 30 km (18.6 mi) in the area between KP and KI.

Group IV

Scenarios in this group include hypothetical ruptures located offshore of the AP, southwest of Kodiak. This is the area of the 1938 and 2021 ruptures. Tsunamis generated by earthquakes in this region will enter Cook Inlet through Shelikof Strait (fig. 1). Scenarios 11 and 12 are based on the results of the sensitivity study for southern scenarios described in Suleimani and others (2023). The proposed slip distributions and vertical coseismic deformations for scenarios 11–13 are shown in figure 7K–M.

Scenario 11: M$_W$ 8.9 earthquake in the KI–AP region: maximum slip at a depth of 15–25 km (9.3–15.5 mi).	The depth of maximum slip corresponds to the depth of sensitivity case C for southern scenarios. The slip skewness parameter, q, is set to 0.5 (bell-shaped curve is not skewed) to model the maximum slip of 36.9 m (121 ft) at a depth of 20 km (12.4 mi).

Scenario 12: M$_W$ 8.8 earthquake in the KI–AP region: maximum slip at a depth of 25–35 km (15.5–21.7 mi).	The depth of maximum slip corresponds to the depth of sensitivity case D for southern scenarios. The slip skewness parameter, q, is set to 0.5 (bell-shaped curve is not skewed) to model the maximum slip of 37 m (121.4 ft) at a depth of 30 km (18.6 mi).

Scenario 13: M$_W$ 9.0 earthquake offshore AP region: SAFRR scenario.	The USGS Science Application for Risk Reduction (SAFRR) project, in collaboration with NOAA and State of California agencies, has developed a plausible hypothetical tsunami scenario (Kirby and others, 2013) to describe the impacts of a tsunami generated by an earthquake in the AP region (Ross and Jones, 2013). The USGS Tsunami Source Working Group defined the scenario source as a M$_W$ 9.0 earthquake like the Tohoku 2011 event, but between the Shumagin Islands and Kodiak Island. The rupture area, represented by 56 subfaults, is about 350 x 200 km (217.5 x 124.3 mi), with an average slip of 15.7 m (51.51 ft) and a maximum slip of 75 m (246.1 ft). Larger values of slip are located near the trench, as was the case with the Tohoku earthquake.

Group V

Ryan and others (2012), and later Kirby and others (2013), compared the Alaska and Tohoku megathrust margins and suggested that a hypothetical rupture in the Alaska–Aleutian subduction zone might propagate to shallow depths as it did in the M_W 9.0 Tohoku earthquake. Shallow fault rupture at the Tohoku margin resulted in a complex mix of blind (concealed) fault-bend folding along the fault length and surface-breaching rupture of the seafloor—both of which contributed to a significant seafloor disturbance. Multibeam bathymetry in the eastern part of the Aleutian megathrust suggests that the Alaska plate margin has similar mixed-behavior shallow ruptures.

Recently, Butler and others (2014) described a layer of sand discovered in the Makauwahi sinkhole on the island of Kaua'i, Hawai'i. The origin of this layer was presumed to be inundation of the sinkhole by a giant paleotsunami following a M_W 9+ earthquake in the eastern Aleutian Islands. Butler (2012) provides an in-depth examination of previous great Aleutian earthquakes and tsunamis impacting Hawai'i. In subsequent research, Butler (2014) considered several hypothetical events with a 35 m (114.8 ft) displacement on the megathrust and up to a 50 m (164 ft) displacement near the trench.

Scenarios 14 and 15 simulate hypothetical ruptures in the eastern part of the Alaska–Aleutian megathrust where the updip and downdip limits of the rupture are between 0 km and 30–40 km (18.6–24.8 mi), respectively. However, we account for the possibility that the slip in the earthquake rupture may be concentrated at the shallowest depths of the plate interface and may breach the sea floor at the trench. We construct scenario 14 with modeled fault slip extending to the shallowest part of the megathrust. The proposed slip distributions and vertical coseismic deformations for scenarios 14 and 15 are shown in figure 7N and O.

Scenario 14: M_W 9.3 earthquake with 50 m (164 ft) of maximum slip close to the trench	The depth of maximum slip corresponds to that of the combination of sensitivity cases A and B. The slip skewness parameter, q, is set to 0.25 (bell-shaped curve skewed toward the trench) to model the maximum slip of 50 m (115 ft) at a depth of 10 km (6.2 mi), and then slip gradually reduces to about 10 m (33 ft) at 30 km (18.6 mi) depth. This scenario was used in previous tsunami inundation mapping reports (for example, Suleimani and others, 2013, 2016; Nicolsky and others, 2017, 2018).
Scenario 15: M_W 9.3 earthquake with 35 m (114.8 ft) of maximum slip in most of the rupture	In this scenario, like Butler (2014), we assume 35 m (114.8 ft) of slip for nearly the entire rupture patch between the 5 km (3.1 mi) and 35 km (21.7 mi) depth contours, with slip decreasing both toward the trench and to the deeper parts of the rupture. A similar scenario was proposed in the tsunami modeling study for Kodiak (scenario 8 of Suleimani and others, 2017).

Group VI

Scenario 16: Rupture of the Cascadia subduction zone, including the entire megathrust between British Columbia and northern California	Scenario 16 considers a hypothetical tsunami generated along the coast of the Pacific Northwest US—relatively distant from the Kenai Peninsula. Although a rupture of the Cascadia subduction zone is not a worst-case scenario for the coast of Southcentral Alaska, this scenario is included for the sake of community preparedness. This scenario is the same as scenario 16 in the tsunami modeling studies for King Cove and Cold Bay (Suleimani and others, 2016). The slip distribution model for this scenario is shown in figure 10 of Wang and others (2003). The vertical coseismic deformations for scenario 16 are shown in figure 7P.

MODELING RESULTS

We modeled water dynamics for each of the previously described scenarios summarized in table 2. The extent of inundation and flow depths were calculated only for the level 4 high-resolution grids. Map sheets 1–4 show the maximum composite extent of inundation for all scenarios, and the maximum composite flow depths over dry land. Refer to the "Grid Development and Data Sources" section of this report for a description of how the composite flow depth maps and the composite tsunami inundation lines are generated from multiple scenarios. The calculated extent of inundation accounts for regional coseismic deformation in Cook Inlet.

First, we analyze the extent of tsunami inundation for all scenarios, organizing them by scenario groups. Then for every community, we select the scenario in each group that results in the largest inundation zone and plot the corresponding inundation lines (figs. 8–11). Scenario 15 results in the worst overall inundation in all communities, followed by scenarios 1 and 6 for Anchor Point, scenarios 7 and 10 for Kenai, scenarios 6 and 10 for Ninilchik, and scenarios 8 and 10 for Tyonek. Since these scenarios are from different groups, it demonstrates that sizable tsunami effects could be produced by coseismic slip at different depths of the subduction interface. Scenario 16, the megathrust earthquake in

the Cascadia subduction zone, resulted in the least amount of inundation in all communities. Scenarios 1, 6, 7, 8, 10, and 15 result in the largest inundation zones; therefore, they have a sizable contribution to the composite maps.

Time Series

The arrival time of the first wave, the maximum wave amplitude, and the duration of wave action are all important factors that should be considered by emergency managers during evacuation planning. Therefore, we supplement the inundation maps with time series of modeled water level and velocity dynamics at certain locations in Cook Inlet. Appendices A–D contain plots of sea level and velocity time series for selected scenarios in Anchor Point, Kenai, Ninilchik, and Tyonek, respectively. These selected scenarios are those that result in maximum inundation in each scenario group for a community. For each location—shown by a number in figures A1, B1, C1, and D1—we plot the sea level and water velocity in figures A2, B2, C2, and D2, respectively.

In all plots in appendices A–D, zero time corresponds to the time at which the earthquake occurs. The pre-earthquake elevation/depth with respect to MHHW is stated for each location. The post-earthquake elevation/depth corresponding to the MHHW datum is also listed for each scenario in tables A1, B1, C1, and D1. To show the height
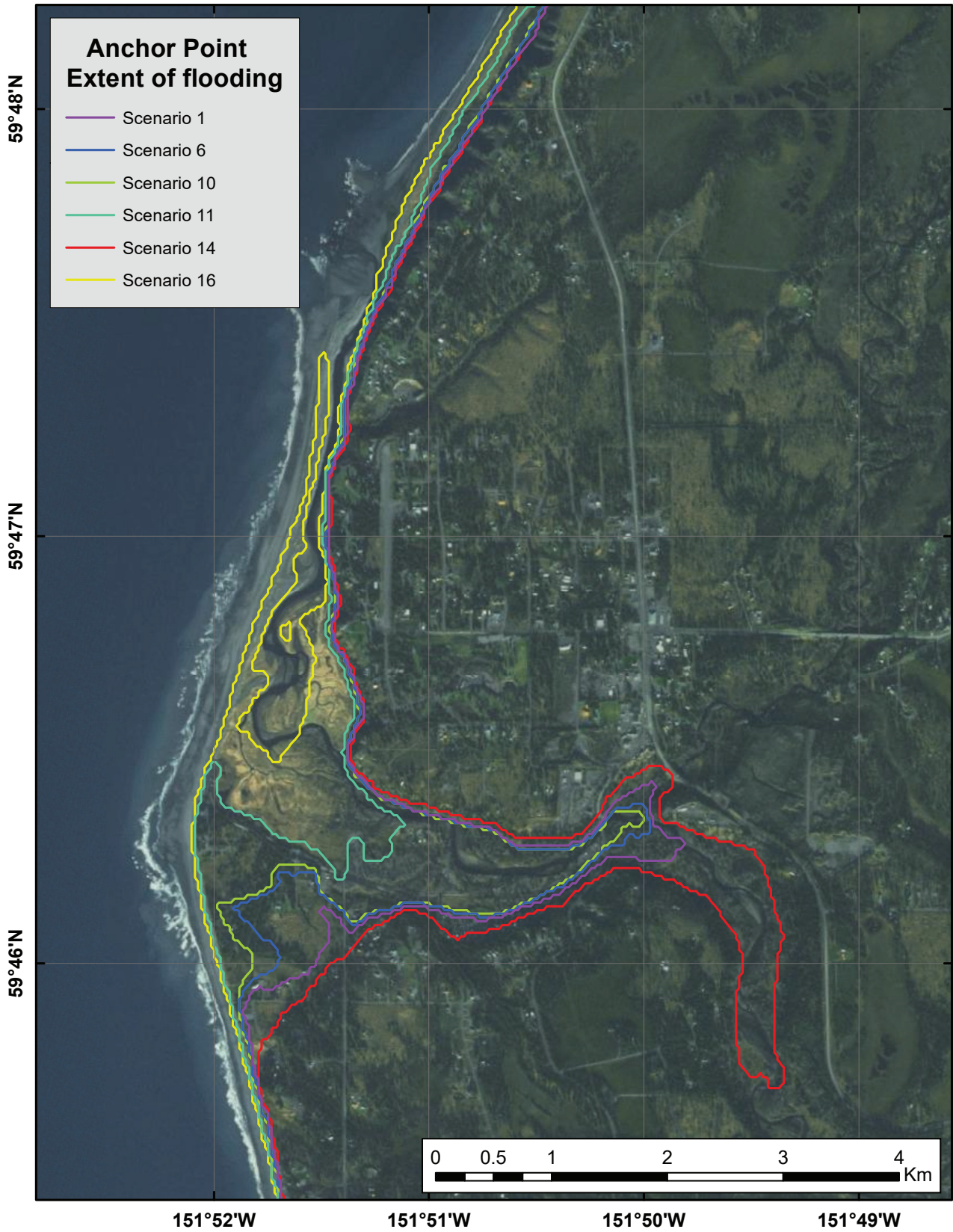
Figure 8. Tsunami inundation in Anchor Point for the worst-case scenarios from each scenario group.
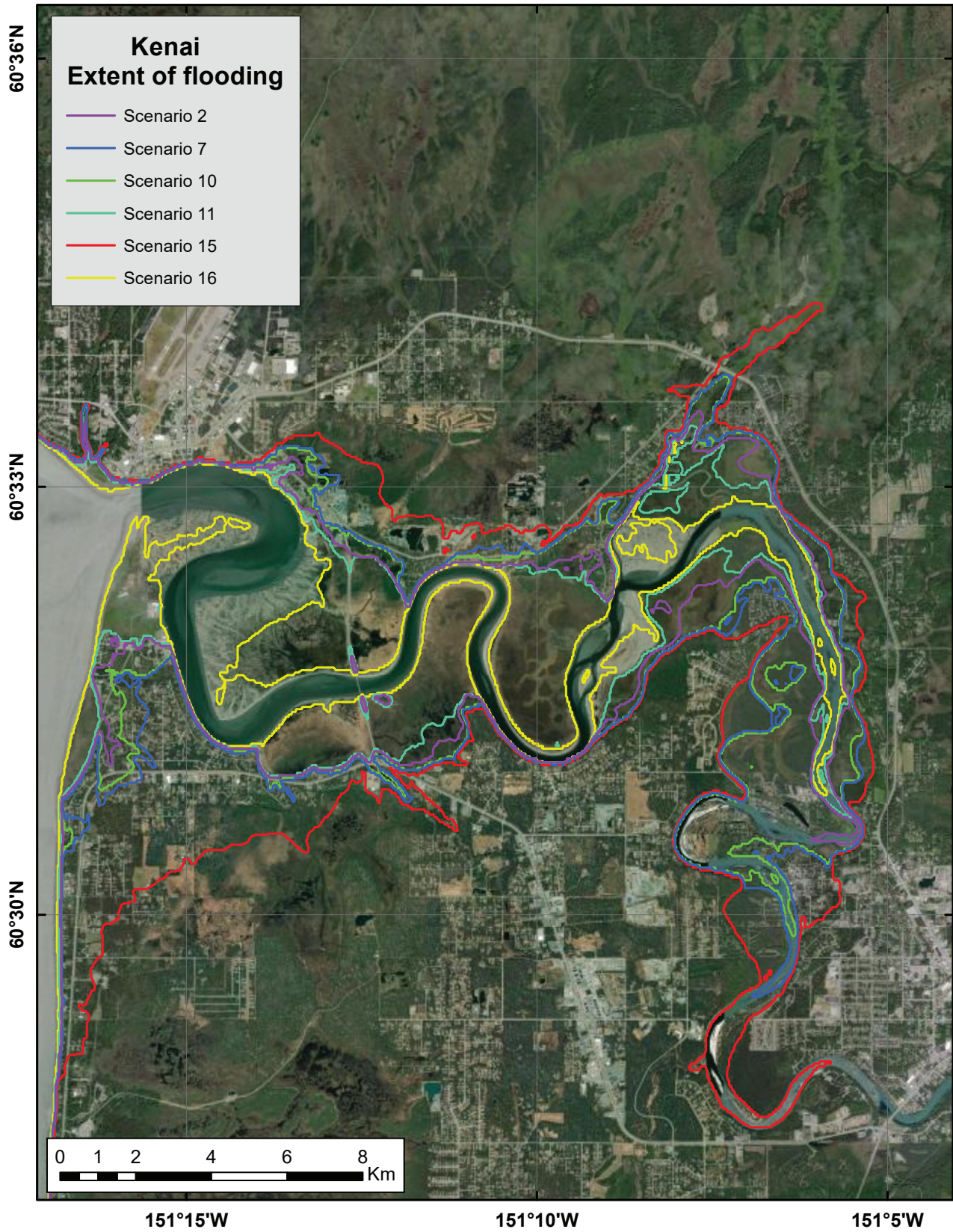
Figure 9. Tsunami inundation in Kenai for the worst-case scenarios from each scenario group.
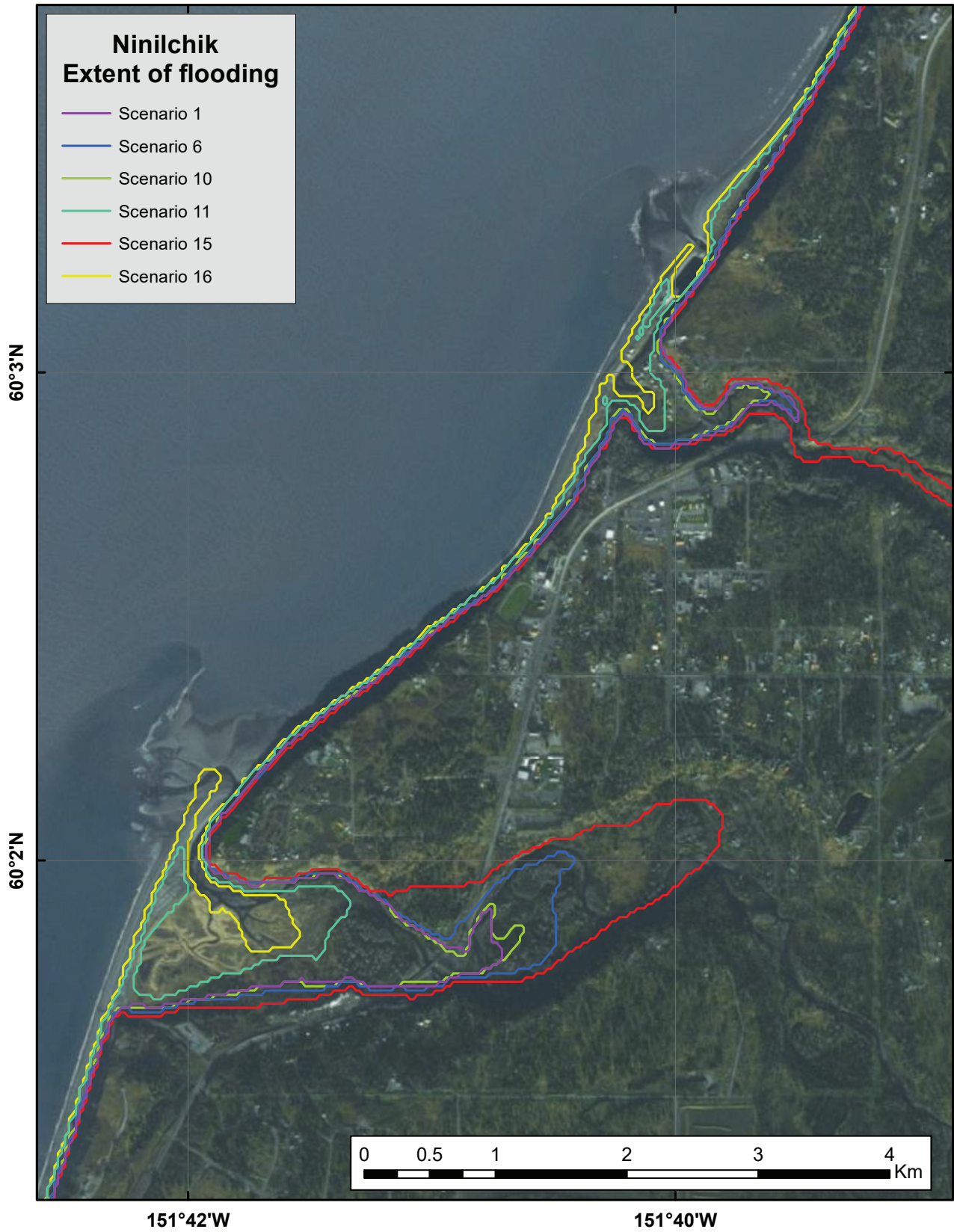
Figure 10. Tsunami inundation in Ninilchik for the worst-case scenarios from each scenario group.

Figure 11. Tsunami inundation in Tyonek for the worst-case scenarios from each scenario group.

of arriving tsunamis for offshore locations we use a vertical datum with a zero-mark corresponding to the pre-earthquake sea level. Velocity was computed only where the water depth is greater than 0.3 m (1.0 ft). The velocity magnitude is calculated as water flux divided by water depth; thus, the uncertainty can be large when the water depth is small.

The maximum water level values for all considered scenarios are listed in tables A2, B2, C2, and D2, and maximum velocity values are given in tables A3, B3, C3, and D3.

SOURCES OF ERRORS AND UNCERTAINTIES

The hydrodynamic model used to calculate propagation and run-up of tectonic tsunamis is a nonlinear, flux-formulated, shallow-water model (Nicolsky and others, 2011b) that passed the verification and validation tests required for numerical codes used to produce tsunami inundation maps (Synolakis and others, 2007; NTHMP, 2012). The spatial resolution of the grid used to calculate tsunami inundation in Cook Inlet communities is about 14 m (46 ft) and satisfies NOAA minimum recommended requirements for computation of tsunami inundation (NTHMP, 2010). Although this resolution is high enough to describe major relief features, small topographic features, buildings, and other facilities cannot be resolved accurately by the existing model. We also note that uncertainty in grid-cell elevation/depth propagates into the modeling results and eventually contributes to horizontal uncertainty in the location of the inundation line.

Another contribution to this uncertainty is the paucity of data in the intertidal zone. However, no established practices exist to directly propagate the digital elevation model uncertainty into the uncertainty of the inundation line (Hare and others, 2011). The direction of the incoming waves, their amplitudes, and times of arrival are primarily determined by displacements of the ocean in the source area. Therefore, the inundation modeling results for local sources are especially sensitive

to the fine structure of the tsunami source. The modeling process is highly sensitive to errors when the complexity of the source function is combined with its proximity to the coastal zone.

Most of the errors/uncertainties in the numerical predictions originate from the tsunamigenic earthquake sources used in the numerical models. Our assessment of potential earthquake scenarios is not exhaustive and represents a best estimate of the locations and sizes of potential tsunami-generating events. It is possible that other unrecognized earthquake scenarios or slope failures (both subaerial and submarine) could present hazards to populated locations in lower Cook Inlet. However, the scenarios presented in this report are intended to cover the range of potential situations about which the communities should be aware.

SUMMARY

We present results of numerical modeling of earthquake-generated tsunamis for four communities in Cook Inlet: Anchor Point, Kenai, Ninilchik, and Tyonek. The hypothetical tsunamigenic earthquakes used in this report are considered worst-case, maximum-possible slip scenarios for the eastern end of the Alaska–Aleutian megathrust. Each scenario represents a unique set of carefully selected geologic conditions (including rupture location and the amount of slip on the plate interface), and while these events are plausible, we make no attempt to estimate the likelihood that these events may occur in the near or distant geologic future. Our goal is to identify potential hazards to the communities to reduce impacts in future worst-case events.

A hypothetical earthquake with maximum slip distributed between depths of 5 and 22 km (3.1 and 13.7 mi) results in "worst case" tsunami inundation for all communities. The maximum predicted overland flow depths for low-lying coastal areas (i.e., tidal mudflats) reach 10 m (32.8 ft) with currents as strong as 12 m/sec (23.4 knots). Dangerous wave activity is expected to last for at least 24 hours after the hypothetical worst-case earthquakes.

Map sheets 1–6, which show the potential extent of inundation and the tsunami flow depths, have been completed using the best information available and are believed to be accurate; however, their preparation required many assumptions. We considered several tsunami scenarios and have provided an estimate of maximum credible tsunami inundation. Actual conditions during a tsunami event may vary from those considered, so the accuracy of predictions based on the modeling presented in this report cannot be guaranteed. The limits of inundation shown should only be used as a guideline for emergency planning and response action. Actual inundated areas will depend on specifics of earthquake deformation, ongoing and future on-land and offshore construction, and tide level, and may differ from areas shown on the maps. The information on these maps is intended to assist state and local agencies in planning for emergency evacuation and tsunami response actions in the event of a major tsunamigenic earthquake. Because these earthquake scenarios do not incorporate probabilities of occurrence, the results are not intended for land-use regulation or building-code development.

ACKNOWLEDGMENTS

REFERENCES

Butler, Rhett, 2012, Re-examination of the potential for great earthquakes along the Aleutian island arc with implication for tsunamis in Hawai'i: Seismological Research Letters, v. 83, no. 1, p. 30–39. doi.org/10.1785/gssrl.83.1.29

———2014, Great Aleutian tsunamis: Honolulu, Hawai'i, University of Hawai'i at Manoa, Hawai'i Institute of Geophysics & Planetology, Peer-Reviewed Report HIGP-2014-1, 170 p.

Butler, Rhett, Burney, David, and Walsh, David, 2014, Paleotsunami evidence on Kaua'i and numerical modeling of a great Aleutian tsunami: Geophysical Research Letters, v. 41, no. 19, p. 6,795–6,802. doi.org/10.1002/2014GL061232

Department of Commerce, Community, and Economic Development (DCCED)/Division of Community and Regional Affairs (DCRA), 2015, Community Database Online. dcra-cdo-dcced.opendata.arcgis.com/

Dunbar, P.K., and Weaver, C.S., 2008, U.S. states and territories national tsunami hazard assessment—Historical record and sources for waves: Technical Report, National Oceanic and Atmospheric Administration and U.S. Geological Survey, 59 p. repository.library.noaa.gov/view/noaa/47448

Fine, I.V., Thomson, R.E., Lupton, L.M., and Mundschutz, Stephen, 2018a, Numerical modeling of an Alaska 1964-type tsunami at the Canadian Coast Guard Base in Seal Cove, British Columbia: Canadian Technical Report of Hydrography and Ocean Sciences 321, Ocean Sciences Division, Fisheries and Oceans Canada, Institute of Ocean Sciences, Sidney, British Columbia.

———2018b, Numerical modeling of an Alaska 1964-type tsunami at the Canadian Coast Guard Base in Victoria, British Columbia: Canadian Technical Report of Hydrography and Ocean Sciences 323, Ocean Sciences Division, Fisheries and Oceans Canada, Institute of Ocean Sciences, Sidney, British Columbia.

Freund, L.B., and Barnett, D.M., 1976, A two-dimensional analysis of surface deformation due to dip-slip faulting: Bulletin of the Seismological Society of America, v. 66, no. 3, p. 667–675.

Geist, E.L., and Parsons, Tom, 2006, Probabilistic analysis of tsunami hazards: Natural Hazards, v. 37, no. 3, p. 277–314. doi.org/10.1007/s11069-005-4646-z

Hare, Rob, Eakins, B.W., and Amanate, Christopher, 2011, Modelling bathymetric uncertainty: International Hydrographic Review, p. 31–42. journals.lib.unb.ca/index.php/ihr/article/view/20888

Hayes, Gavin, 2018, Slab2 – A comprehensive subduction zone geometry model: U.S. Geological Survey data release. doi.org/10.5066/F7PV6JNV

Johnson, J.M., Satake, Kenji, Holdahl, S.R., and Sauber, Jeanne, 1996, The 1964 Prince William Sound earthquake—Joint inversion of tsunami waveforms and geodetic data: Journal of Geophysical Research, v. 101, no. B1, p. 523–532. doi.org/10.1029/95JB02806

Kanamori, Hiroo, 1970, The Alaska earthquake of 1964: Radiation of long-period surface waves and source mechanism: Journal of Geophysical Research, v. 75, no. 26, p. 5,029–5,040. doi.org/10.1029/JB075i026p05029

Kelsey, H.M., Witter, R.C., Engelhart, S.E., Briggs, Richard, Nelson, Alan, Haeussler, P.J., and Corbett, D.R., 2015, Beach ridges as paleoseismic indicators of abrupt coastal subsidence during subduction zone earthquakes, and implications for Alaska–Aleutian subduction zone paleoseismology, southeast coast of the Kenai Peninsula, Alaska: Quaternary Science Reviews, v. 113, p. 147–158. doi.org/10.1016/j.quascirev.2015.01.006

Kirby, Stephen, Scholl, David, von Huene, Roland, and Wells, Ray, 2013, Alaska earthquake source for the SAFRR tsunami scenario, chapter B, in Ross, S.L., and Jones, L.M., eds., The SAFRR (science application for risk reduction) tsunami scenario: U.S. Geological Survey Open-File Report 2013–1170, 40 p. pubs.usgs.gov/of/2013/1170/b/

Lander, J.F., 1996, Tsunamis affecting Alaska, 1737–1996: Boulder, Colorado, National Oceanic and Atmospheric Administration, National Geophysical Data Center (NGDC), Key to Geophysical Research Documentation, v. 31, 155 p.

Larsen, C.F., Motyka, R.J., Freymueller, J.T., Echelmeyer, K.A., and Ivins, E.R., 2004, Rapid uplift of southern Alaska caused by recent ice loss: Geophysical Journal International, v. 158, no. 3, p. 1,118–1,133. doi.org/10.1111/j.1365-246X.2004.02356.x

Moss, R.E.S., and Travasarou, Thaleia, 2006, Tsunamigenic probabilistic fault displacement hazard analysis for subduction zones—Proceedings of the 8th U.S. National Conference on Earthquake Engineering: Earthquake Engineering Research Institute, Paper 238, 9 p.

National Tsunami Hazard Mapping Program (NTHMP), 2010, Guidelines and best practices for tsunami inundation modeling for evacuation planning: National Oceanic and Atmospheric Administration (NOAA), NTHMP Mapping & Modeling Subcommittee.

———2012, Proceedings and results of the 2011 NTHMP Model Benchmarking Workshop: Boulder, CO, U.S. Department of Commerce/NOAA/NTHMP, NOAA Special Report, 436 p.

Nicolsky, D.J., Suleimani, E.N., Combellick, R.A., and Hansen, R.A., 2011a, Tsunami inundation maps of Whittier and western Passage Canal, Alaska: Alaska Division of Geological & Geophysical Surveys Report of Investigation 2011-7, 65 p. doi.org/10.14509/23244

Nicolsky, D.J., Suleimani, E.N., Freymueller, J.T., and Koehler, R.D., 2015, Tsunami inundation maps of Fox Islands communities, including Dutch Harbor and Akutan, Alaska: Alaska Division of Geological & Geophysical Surveys Report of Investigation 2015-5, 67 p., 2 sheets, scale 1:12,500. doi.org/10.14509/29414

Nicolsky, D.J., Suleimani, E.N., Haeussler, P.J., Ryan, H.F., Koehler, R.D., Combellick, R.A., and Hansen, R.A., 2013, Tsunami inundation maps of Port Valdez, Alaska: Alaska Division of Geological & Geophysical Surveys Report of Investigation 2013-1, 77 p., 1 sheet, scale 1:12,500. doi.org/10.14509/25055

Nicolsky, D.J., Suleimani, E.N., and Hansen, R.A., 2011b, Validation and verification of a numerical model for tsunami propagation and runup: Pure and Applied Geophysics, v. 168, no. 6, p. 1,199–1,222. doi.org/10.1007/s00024-010-0231-9

Nicolsky, D.J., Suleimani, E.N., and Koehler, R.D., 2014, Tsunami inundation maps of Cordova and Tatitlek, Alaska: Alaska Division of Geological & Geophysical Surveys Report of Investigation 2014-1, 49 p. doi.org/10.14509/27241

———2016, Tsunami inundation maps for the communities of Chignik and Chignik Lagoon, Alaska: Alaska Division of Geological & Geophysical Surveys Report of Investigation 2016-8, 48 p., 2 sheets, scale 1:12,500. doi.org/10.14509/29675

Nicolsky, D.J., Suleimani, E.N., Koehler, R.D., and Salisbury, J.B., 2017, Tsunami inundation maps for Juneau, Alaska: Alaska Division of Geological & Geophysical Surveys Report of Investigation 2017-9, 66 p., 5 sheets. doi.org/10.14509/29741

Nicolsky, D.J., Suleimani, E.N., and Salisbury, J.B., 2018, Tsunami inundation maps for Skagway and Haines, Alaska: Alaska Division of Geological & Geophysical Surveys Report of Investigation 2018-2, 69 p., 3 sheets. doi.org/10.14509/30029

Okada, Yoshimitsu, 1985, Surface deformation due to shear and tensile faults in a half-space: Bulletin of the Seismological Society of America, v. 75, no. 4, p. 1,135–1,154.

Oppenheimer, Michael, Glavovic, B.C., Hinkel, Jochen, van de Wal, Roderik, Magnan, A.K., Abd-Elgawad, Amro, Cai, Rongshuo, Cifuentes-Jara, Miguel, DeConto, R.M., Ghosh, Tuhin, Hay, John, Isla, Federico, Marzeion, Ben, Meyssignac, Benoit, and Sebesvari, Zita, 2019, Sea level rise implications for low-lying islands, coasts and communities, in Pörtner, H.-O., Roberts, D.C., Masson-Delmotte, V., Zhai, P., Tignor, M., Poloczanska, E., Mintenbeck, K., Alegría, A., Nicolai, M., Okem, A., Petzoid, J., Rama, B., and Weyer, N.M., eds., IPCC Special Report on the ocean and cryosphere in a changing climate. www.ipcc.ch/srocc/chapter/chapter-4-sea-level-rise-and-implications-for-low-lying-islands-coasts-and-communities/

Papazachos, B.C., Scordilis, E.M., Panagiotopoulos, D.G., Papazachos, C.B., and Karakaisis, G.F., 2005, Global relations between seismic fault parameters and moment magnitude of earthquakes: Bulletin of the Geological Society of Greece, v. 36, p. 1,482–1,489.

Plafker, George, Kachadoorian, Reuben, Eckel, E.B., and Mayo, L.R., 1969, Effects of the earthquake of March 27, 1964, on various communities: U.S. Geological Survey Professional Paper 542-G, 50 p. pubs.usgs.gov/pp/0542g/

Rabinovich, A.B., Thomson, R.E., Krassovski, M.V., Stephenson, F.E., and Sinnott, D.C., 2019, Five great tsunamis of the 20th century as recorded on the coast of British Columbia: Pure and Applied Geophysics, v. 176, p. 2,887–2,924. doi.org/10.1007/s00024-019-02133-3

Ross, S.L., and Jones, L.M., eds., 2013, The SAFRR Tsunami Scenario: U.S. Geological Survey Open-File Report 2013–1170, 897 p. pubs.usgs.gov/of/2013/1170/

Ryan, Holly, von Huene, Roland, Scholl, Dave, and Kirby, Steve, 2012, Tsunami hazards to U.S. coasts from giant earthquakes in Alaska: Eos American Geophysical Union, v. 93, no. 19, 185 p.

Shennan, Ian, Barlow, Natasha, and Combellick, R.A., 2008, Paleoseismological records of multiple great earthquakes in south-central Alaska—A 4,000 year record at Girdwood, in Freymueller, J.T., Haeussler, P.J., Wesson, R.L, and Ekström, G., eds., Active tectonics and seismic potential of Alaska: American Geophysical Union Geophysical Monograph 179, p. 185–199.

Shirzaei, Manoochehr, Freymueller, Jeffrey, Törnqvist, T.E., Galloway, D.L., Dura, Tina, and Minderhoud, P.S.J., 2021, Measuring, modelling and projecting coastal land subsidence: Nature Reviews Earth & Environment, v. 2, p. 40–58. doi.org/10.1038/s43017-020-00115-x

Suleimani, E.N., Salisbury, J.B., and Nicolsky, D.J., 2023, Tsunami inundation maps of Anchorage and upper Cook Inlet, Alaska: Alaska Division of Geological & Geophysical Surveys Report of Investigation 2023-2, 56 p., 9 sheets. https://doi.org/10.14509/31018

Suleimani, E.N., Nicolsky, D.J., and Koehler, R.D., 2013, Tsunami inundation maps of Sitka, Alaska: Alaska Division of Geological & Geophysical Surveys Report of Investigation 2013-3, 76 p., 1 sheet, scale 1:250,000. doi.org/10.14509/26671

———2015, Tsunami inundation maps of Elfin Cove, Gustavus, and Hoonah, Alaska: Alaska Division of Geological & Geophysical Surveys Report of Investigation 2015-1, 79 p. doi.org/10.14509/29404

———2017, Updated tsunami inundation maps of the Kodiak area, Alaska: Alaska Division of Geological & Geophysical Surveys Report of Investigation 2017-8, 38 p., 10 sheets. doi.org/10.14509/29740

Suleimani, E.N., Nicolsky, D.J., Koehler, R.D., Freymueller, J.T., and Macpherson, A.E., 2016, Tsunami inundation maps for King Cove and Cold Bay communities, Alaska: Alaska Division of Geological & Geophysical Surveys Report of Investigation 2016-1, 73 p., 2 sheets, scale 1:12,500. doi.org/10.14509/29565

Suleimani, E.N., Nicolsky, D.J., and Salisbury, J.B., 2019, Updated tsunami inundation maps for Homer and Seldovia, Alaska: Alaska Division of Geological & Geophysical Surveys Report of Investigation 2018-5 v. 2, 97 p., 11 sheets. doi.org/10.14509/30095

Suleimani, E.N., Nicolsky, D.J., West, D.A., Combellick, R.A., and Hansen, R.A., 2010, Tsunami inundation maps of Seward and northern Resurrection Bay, Alaska: Alaska Division of Geological & Geophysical Surveys Report of Investigation 2010-1, 47 p., 3 sheets, scale 1:12,500. doi.org/10.14509/21001

Synolakis, C.E., Bernard, E.N., Titov, V.V., Kânoğlu, U., and González, F.I., 2007, Standards, criteria, and procedures for NOAA evaluation of tsunami numerical models: National Oceanic and Atmospheric Administration (NOAA)/Pacific Marine Environmental Laboratory (PMEL) Technical Memorandum OAR PMEL-135, 55 p. www.pmel.noaa.gov/pubs/PDF/syno3053/syno3053.pdf

Wang, Kelin, Sun, Tianhaozhe, Brown, Lonn, Hino, Ryota,Tomita, Fumiaki, Kido, Moyoyuki, Iinuma, Takeshi, Kodaira, Shuichi, and Fujiwara, Toshiya, 2018, Learning from crustal deformation associated with the M9 2011 Tohoku-oki earthquake: Geosphere, v. 14, no. 2, p. 552–571. doi.org/10.1130/GES01531.1

Wang, Kelin, Wells, R.E., Mazzotti, Stephane, Hyndman, R.D., and Sagiya, Takeshi, 2003, A revised dislocation model of interseismic deformation of the Cascadia subduction zone: Journal of Geophysical Research, v. 108, no. B1, p. 2,026–2,038. doi.org/10.1029/2001JB001227

Wang, Taiping, and Yang, Zhaoqing, 2020, A tidal hydrodynamic model for Cook Inlet, Alaska, to support tidal energy resource characterization: Journal of Marine Science and Engineering, v. 8, no. 4. doi.org/10.3390/jmse8040254

Zweck, Chris, Freymueller, J.T., and Cohen, S.C., 2002, Three-dimensional elastic dislocation modeling of the postseismic response to the 1964 Alaska earthquake: Journal of Geophysical Research, v. 107, no. B4. doi.org/10.1029/2001JB000409

APPENDIX A: ANCHOR POINT

Figure A1. Locations of time series points in and around Anchor Point. The longitude and latitude locations of the time series points are listed in table A1.

Figure A2. Time series of water level (left column) and velocity (right column) for selected scenarios at locations shown in figure A1. Elevations of onshore locations and ocean depth at offshore locations are given based on the pre-earthquake MHHW datum.

Point 5
Anchor Point Road

Point 5
Anchor Point Road

Elevation 4.4 m (14.3 ft)

■— Scenario 1   ●— Scenario 6   ▲— Scenario 10   ▲— Scenario 11   ◆— Scenario 14   ■— Scenario 16

Point 6
Anchor River Campground

Point 6
Anchor River Campground

Elevation 5.8 m (19.1 ft)

■— Scenario 1   ●— Scenario 6   ▲— Scenario 10   ▲— Scenario 11   ◆— Scenario 14   ■— Scenario 16

Point 7
Halibut Campground

Point 7
Halibut Campground

Elevation 3.5 m (11.6 ft)

■— Scenario 1   ●— Scenario 6   ▲— Scenario 10   ▲— Scenario 11   ◆— Scenario 14   ■— Scenario 16

Point 8
Boat Launch

Point 8
Boat Launch

Elevation 3.0 m (9.7 ft)

■— Scenario 1   ●— Scenario 6   ▲— Scenario 10   ▲— Scenario 11   ◆— Scenario 14   ■— Scenario 16

Figure A2, continued. Time series of water level (left column) and velocity (right column) for selected scenarios at locations shown in figure A1. Elevations of onshore locations and ocean depth at offshore locations are given based on the pre-earthquake MHHW datum.

Point 9
Anchor Point beach

Point 9
Anchor Point beach

Elevation 1.0 m (3.3 ft)

Scenario 1   Scenario 6   Scenario 10   Scenario 11   Scenario 14   Scenario 16

Point 10
Whiskey Gulch

Point 10
Whiskey Gulch

Elevation 1.5 m (5.0 ft)

Scenario 1   Scenario 6   Scenario 10   Scenario 11   Scenario 14   Scenario 16

Figure A2, continued. Time series of water level (left column) and velocity (right column) for selected scenarios at locations shown in figure A1. Elevations of onshore locations and ocean depth at offshore locations are given based on the pre-earthquake MHHW datum.

Table A1. Location of time series points in and around Anchor Point. The maximum water depth above ground is provided for onshore locations (S), whereas the maximum water level above the pre-earthquake MHHW is provided for offshore (O) locations.

#	Label	S/O	Longitude (°W)	Latitude (°N)	Min. elevation/ depth (m)
1	Cook Inlet	O	-151.921389	59.774722	18.2
2	Seward Circle	S	-151.864444	59.764444	-0.2
3	Kyllonen Campsite	S	-151.863333	59.766389	0.1
4	Kyllonen RV Park	S	-151.860278	59.770833	-0.9
5	Anchor Point Road	S	-151.847778	59.769167	-1.3
6	Anchor River Campground	S	-151.8375	59.770833	0.2
7	Halibut Campground	S	-151.866667	59.771111	-2.1
8	Boat Launch	S	-151.866944	59.773611	-2.7
9	Anchor Point beach	S	-151.836667	59.809722	-4.6
10	Whiskey Gulch	S	-151.821389	59.831944	-4.0

Table A2. Maximum water depth for all tsunami scenarios at time series points in and around Anchor Point.

#	Label	Maximum water depth above ground/sea level (meters)															
		Scenario															
		1	2	3	4	5	6	7	8	9	10	11	12	13	14	15	16
1	Cook Inlet	5.1	4.8	5.7	5.7	3.3	6.7	4.6	5.8	4.0	5.8	2.0	1.7	0.9	8.5	10.0	0.7
2	Seward Circle	2.4	1.5	0.5	0	0	0.9	0	0	0	0.2	0	0	0	5.4	5.0	0
3	Kyllonen Campsite	1.6	0.4	0.2	0	0	0.6	0	0	0	0	0	0	0	5.9	4.7	0
4	Kyllonen RV Park	2.5	1.5	1.2	0.8	0	1.4	0	0.5	0	1.0	0	0	0	6.4	5.6	0
5	Anchor Point Road	3.2	2.0	2.5	1.5	0	2.2	0	1.5	0	1.6	0	0	0	8.5	6.1	0
6	Anchor River Campground	2.4	1.4	1.6	0.6	0	1.0	0	0.5	0	0.7	0	0	0	7.5	4.6	0
7	Halibut Campground	4.4	2.9	2.2	1.9	0	2.4	0.2	1.7	0	2.0	0	0	0	7.9	6.7	0
8	Boat Launch	4.1	3.4	2.7	2.5	0	3.0	0.8	2.2	0.5	2.6	0	0	0	8.4	7.1	0
9	Anchor Point beach	7.9	6.9	4.1	4.1	2.2	5.0	2.9	4.2	3.0	4.2	0.5	0.2	0	9.0	9.2	0
10	Whiskey Gulch	6.6	5.5	3.5	3.5	1.8	4.5	2.4	3.7	2.5	3.5	0	0	0	7.2	8.6	0

Table A3. Maximum water velocities for all tsunami scenarios at time series points in and around Anchor Point.

#	Label	Maximum water velocity (meters/second)															
		Scenario															
		1	2	3	4	5	6	7	8	9	10	11	12	13	14	15	16
1	Cook Inlet	3.1	2.5	1.9	2.3	2.0	2.9	2.2	2.6	1.4	2.3	1.4	1.0	0.6	3.6	4.3	0.5
2	Seward Circle	5.7	4.6	0	0	0	2.1	0	0	0	0	0	0	0	3.9	3.8	0
3	Kyllonen Campsite	2.7	1.4	0	0	0	0.3	0	0	0	0	0	0	0	3.7	2.6	0
4	Kyllonen RV Park	7.9	3.6	3.6	1.4	0	2.1	0	1.5	0	1.6	0	0	0	10.9	5.1	0
5	Anchor Point Road	5.5	3.5	2.4	1.6	0	1.6	0	1.5	0	1.6	0	0	0	7.7	2.9	0
6	Anchor River Campground	4.0	2.6	1.9	0.9	0	0.9	0	0.8	0	1.1	0	0	0	6.6	4.2	0
7	Halibut Campground	6.1	5.1	1.8	1.1	0	2.3	0	1.7	0	1.5	0	0	0	4.8	4.3	0
8	Boat Launch	7.7	6.7	4.6	3.5	0	4.3	2.5	3.9	3.2	3.5	0	0	0	7.3	4.6	0
9	Anchor Point beach	7.4	7.2	1.0	1.1	0.5	1.0	0.7	0.7	0.8	1.0	0.4	0	0	4.8	2.0	0
10	Whiskey Gulch	5.7	5.6	0.9	0.9	0.4	1.1	0.6	0.8	0.6	0.8	0	0	0	3.4	2.7	0

APPENDIX B: KENAI
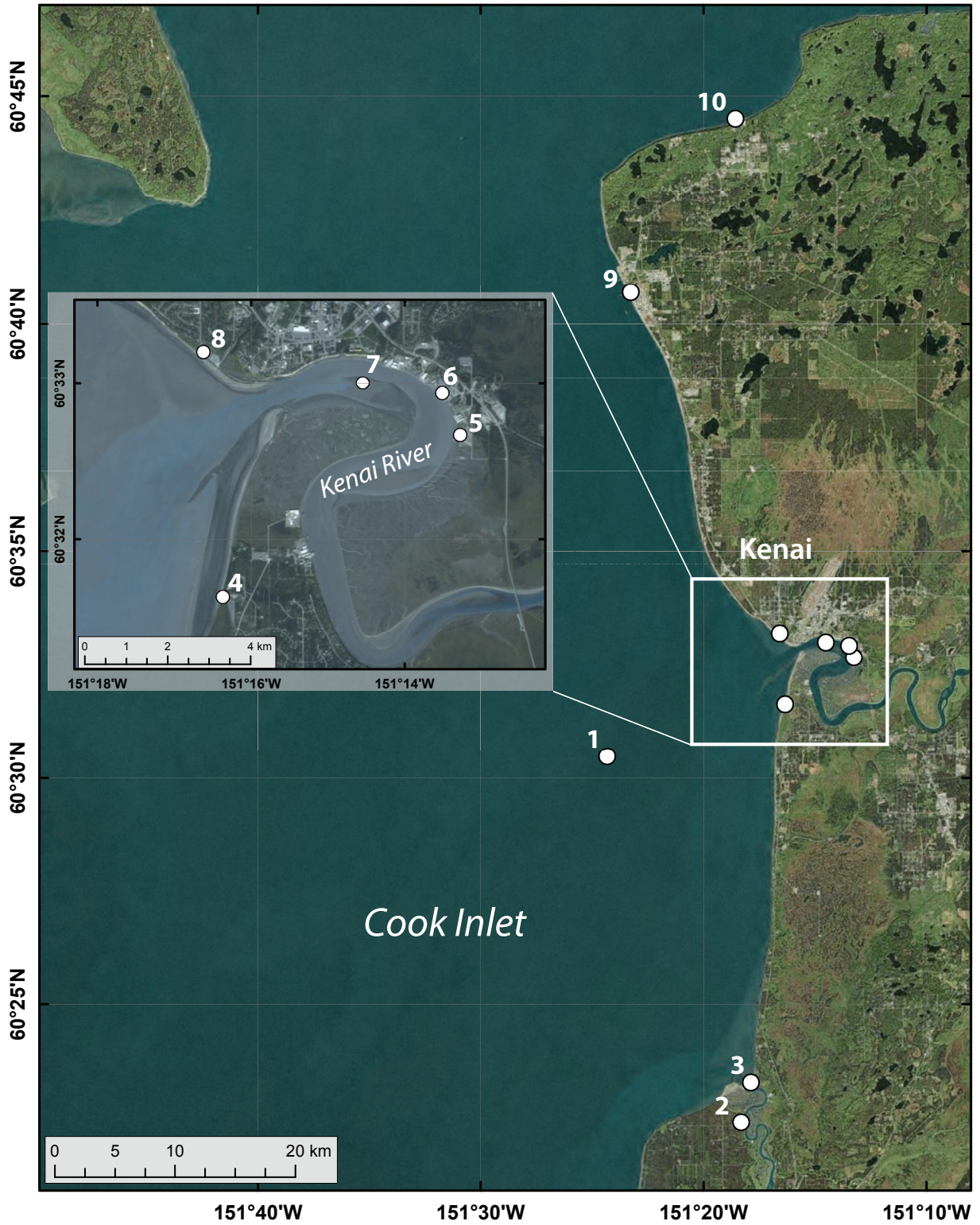
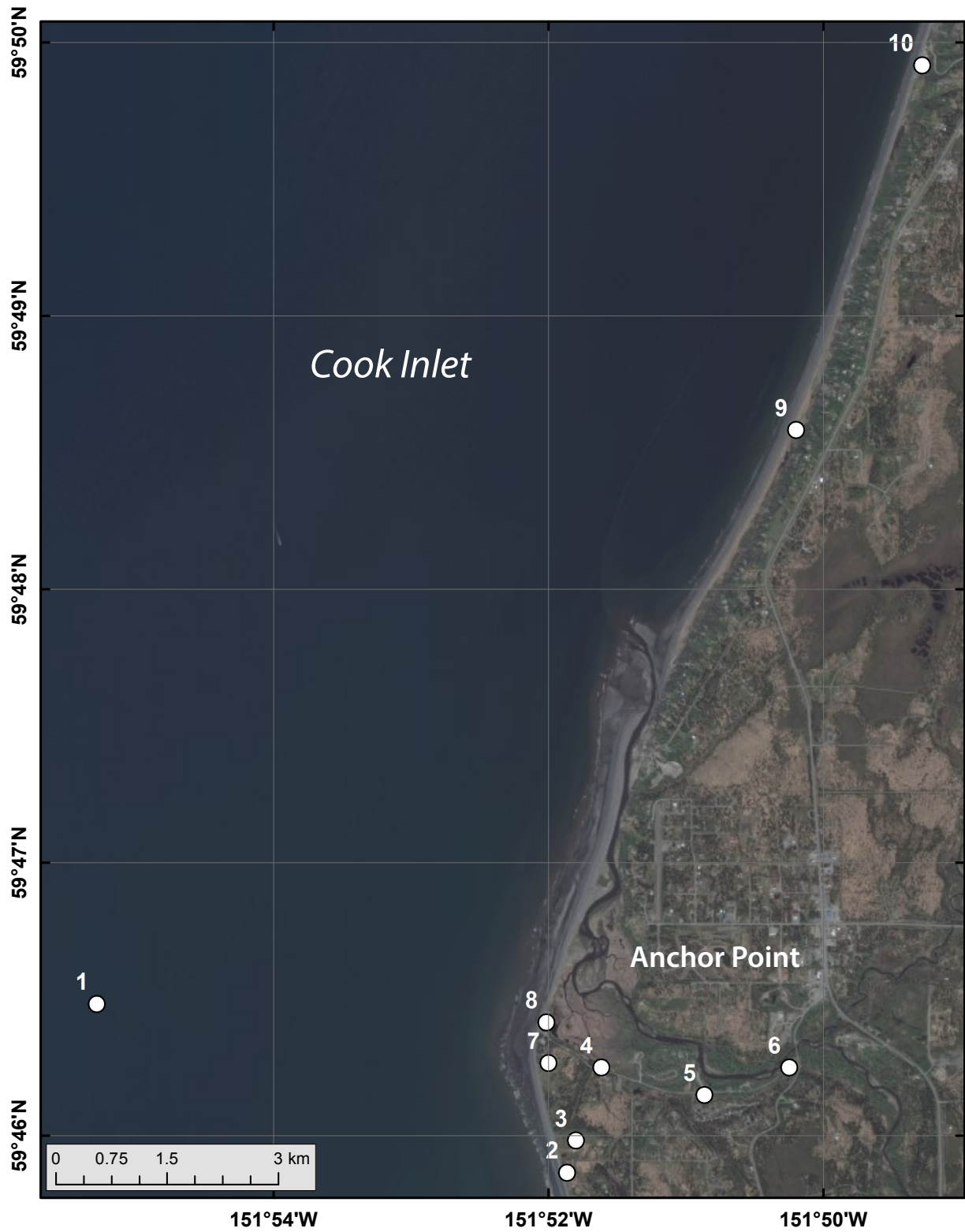**Figure B1.** Locations of time series points in and around Kenai. The longitude and latitude locations of the time series points are listed in table B1.
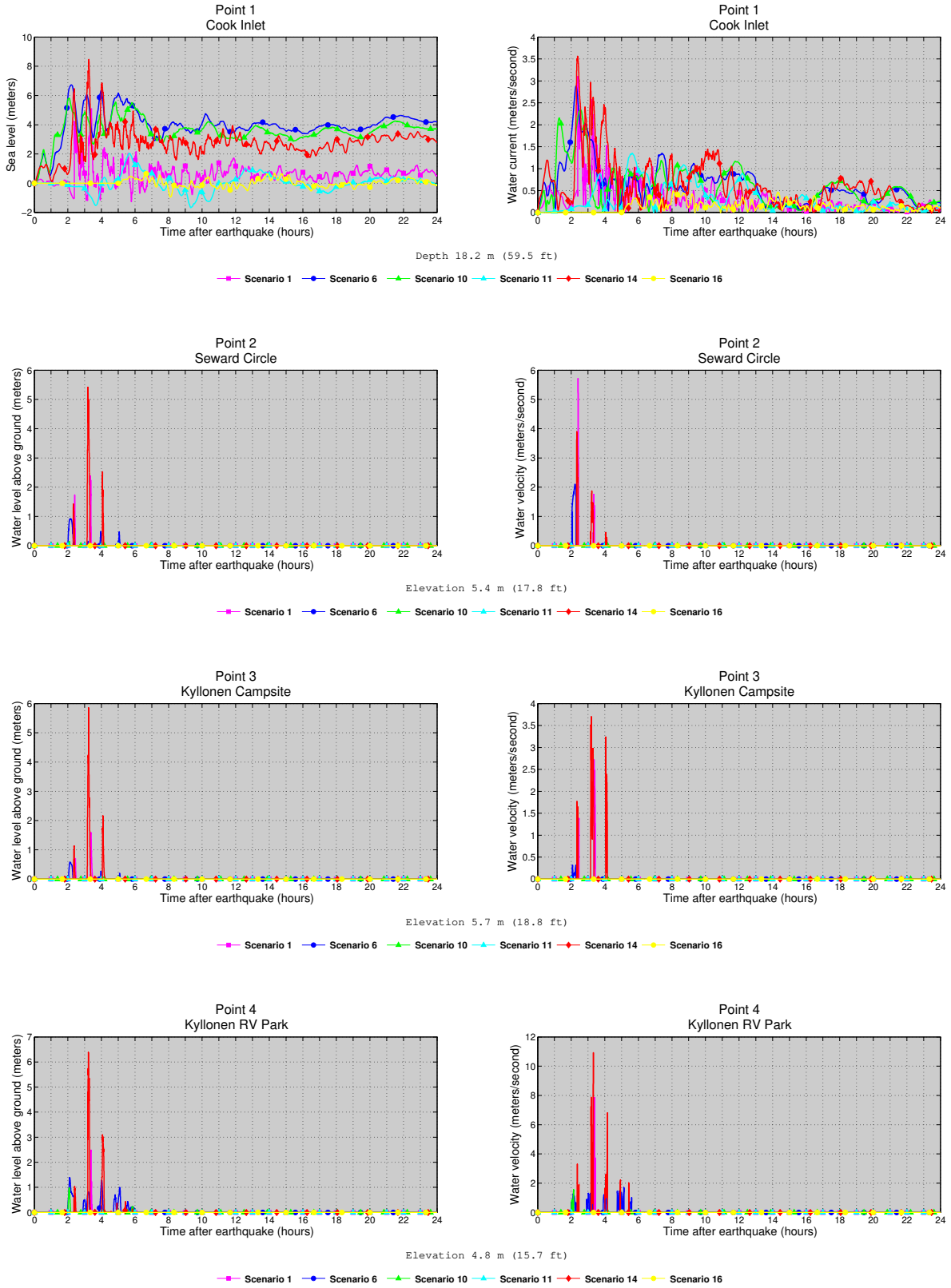
Figure B2. Time series of water level (left column) and velocity (right column) for selected scenarios at locations shown in figure B1. Elevations of onshore locations and ocean depth at offshore locations are given based on the pre-earthquake MHHW datum.
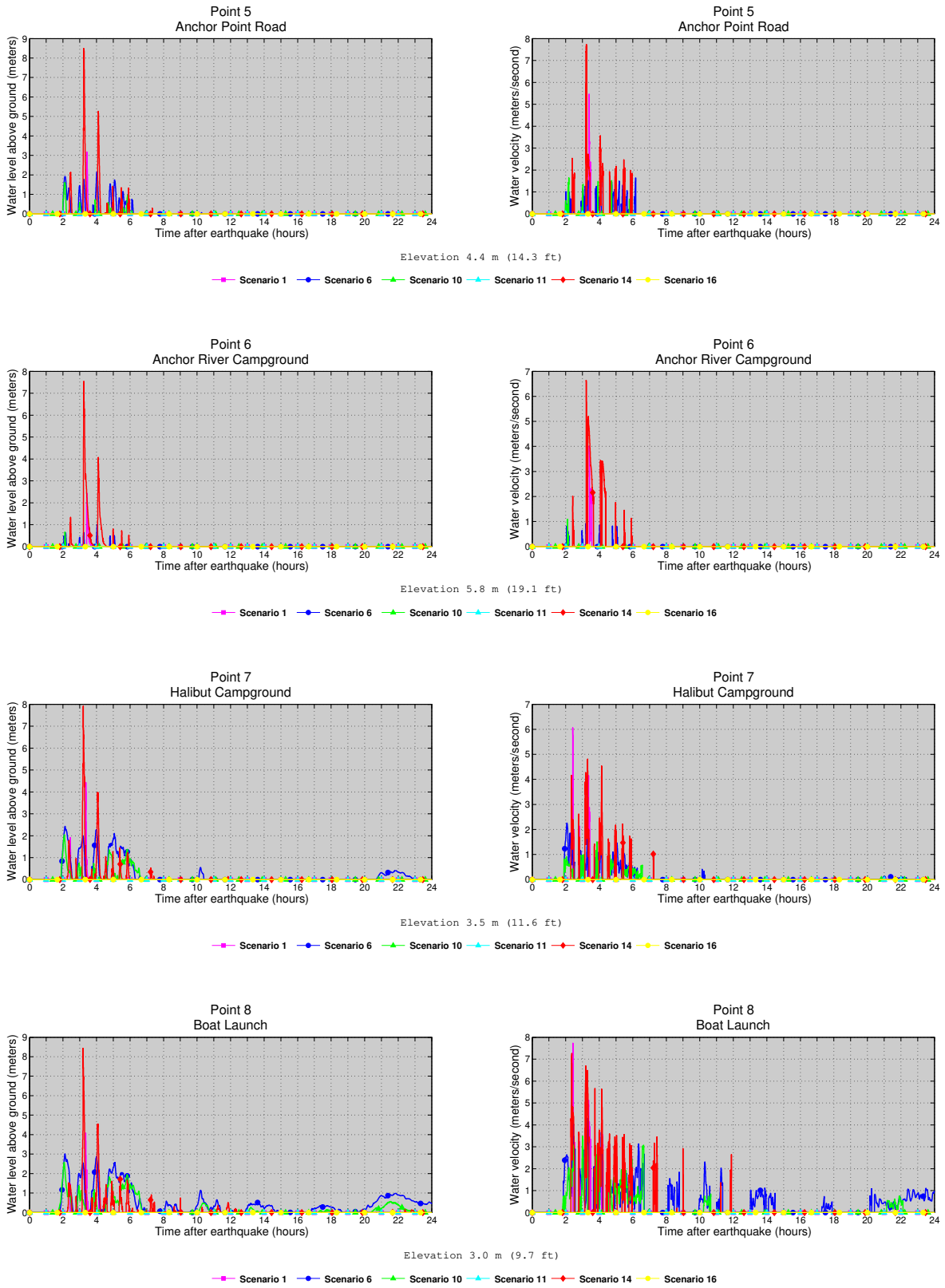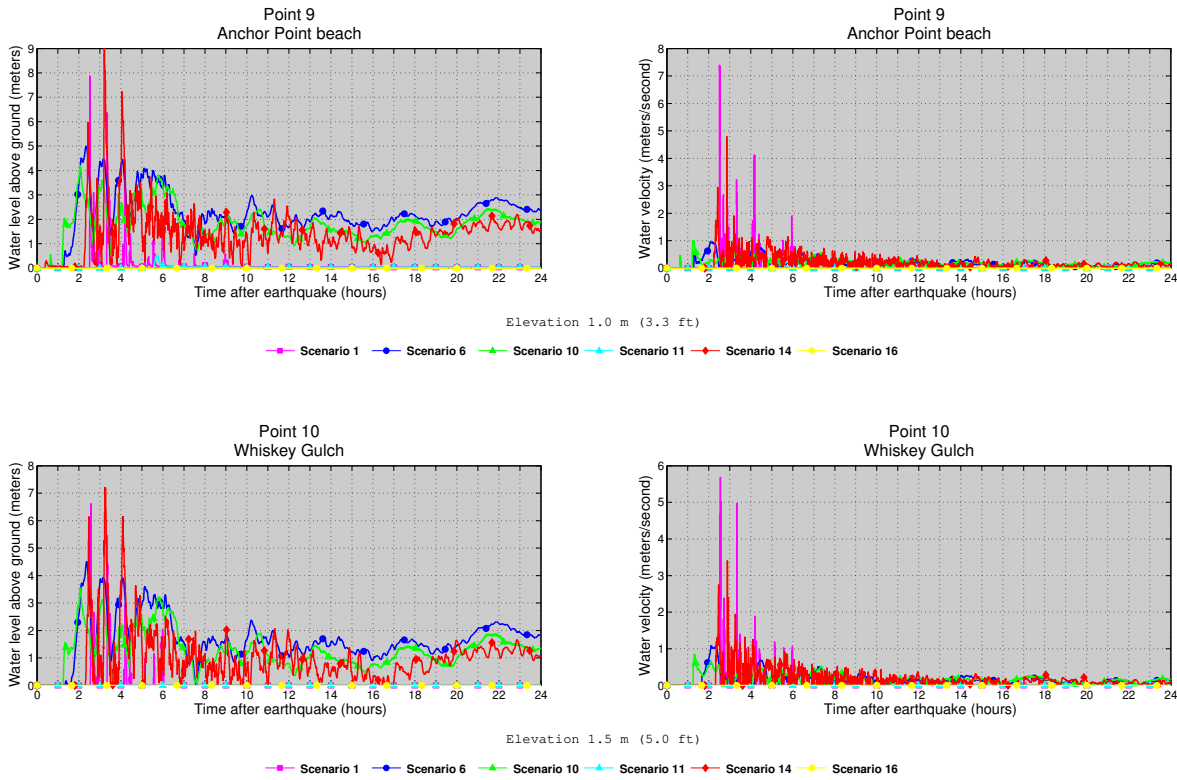
Figure B2, continued. Time series of water level (left column) and velocity (right column) for selected scenarios at locations shown in figure B1. Elevations of onshore locations and ocean depth at offshore locations are given based on the pre-earthquake MHHW datum.

Elevation 27.1 m (89.0 ft)

Elevation 3.3 m (11.0 ft)

Figure B2, continued. Time series of water level (left column) and velocity (right column) for selected scenarios at locations shown in figure B1. Elevations of onshore locations and ocean depth at offshore locations are given based on the pre-earthquake MHHW datum.

Table B1. Location of time series points in and around Kenai. The maximum water depth above ground is provided for onshore locations (S), whereas the maximum water level above the pre-earthquake MHHW is provided for offshore (O) locations.

#	Label	S/O	Longitude (°W)	Latitude (°N)	Min. elevation/ depth (m)
1	Cook Inlet	O	-151.405556	60.508056	19.6
2	Kasilof River Lodge	S	-151.305556	60.373056	-1.3
3	Kasilof Beach	S	-151.298056	60.387778	-3.8
4	South Kenai Beach	S	-151.272778	60.527222	-3.4
5	Kenai Boat Launch	S	-151.221389	60.544444	-4.5
6	Copper River Seafoods	S	-151.225278	60.548889	-4.7
7	Kenai River	O	-151.2425	60.55	5.4
8	Sewer Treatment Plant	S	-151.276944	60.553333	1.1
9	Marathon Corporation	S	-151.388333	60.678333	21.6
10	Offshore Systems	S	-151.309722	60.741667	-2.4

Table B2. Maximum water depth for all tsunami scenarios at time series points in and around Kenai.

#	Label	Maximum water depth above ground/sea level (meters)															
		Scenario															
		1	2	3	4	5	6	7	8	9	10	11	12	13	14	15	16
1	Cook Inlet	3.2	3.4	5.4	5.8	5.5	6.2	6.5	6.1	4.1	5.7	2.4	2.3	1.1	6.9	9.8	0.7
2	Kasilof River Lodge	0	0	0.8	1.3	0.8	2.0	1.8	1.9	1.4	1.3	0	0	0	3.8	5.4	0
3	Kasilof Beach	1.4	1.6	3.2	3.8	3.2	4.1	4.1	4.2	3.5	3.8	0.4	0.3	0	5.8	7.6	0
4	South Kenai Beach	3.0	2.2	3.5	4.5	3.0	3.9	4.6	3.8	2.4	4.2	0.4	0.2	0	5.6	7.6	0
5	Kenai Boat Launch	2.4	2.4	4.2	4.7	4.2	5.1	5.2	5.0	3.3	4.5	1.3	1.0	0	6.6	9.1	0
6	Copper River Seafoods	2.8	2.7	4.6	5.6	4.5	5.4	6.1	5.2	3.6	5.3	1.4	1.1	0	7.2	9.4	0
7	Kenai River	3.2	3.3	5.5	5.9	5.6	6.5	6.8	6.4	4.5	5.8	2.5	2.1	1.1	7.9	10.4	0.7
8	Sewer Treatment Plant	0	0	0	0.7	0	0	1.0	0	0	0.4	0	0	0	1.4	3.4	0
9	Marathon Corporation	0	0	0	0	0	0	0	0	0	0	0	0	0	0	0	0
10	Offshore Systems	0	0	1.0	2.4	1.7	1.8	2.9	2.3	0	2.5	0	0	0	1.5	6.2	0

Table B3. Maximum water velocities for all tsunami scenarios at time series points in and around Kenai.

| #	Label	Maximum water velocity (meters/second)															
		Scenario															
		1	2	3	4	5	6	7	8	9	10	11	12	13	14	15	16
1	Cook Inlet	1.4	1.4	1.9	1.7	1.2	1.8	1.7	1.6	0.9	1.6	1.0	0.9	0.4	2.1	2.3	0.4
2	Kasilof River Lodge	0	0	1.1	1.7	1.6	1.4	1.7	1.7	1.6	1.7	0	0	0	2.9	1.5	0
3	Kasilof Beach	4.4	4.5	5.5	5.5	3.1	4.8	5.7	4.0	5.0	5.4	2.0	0.8	0	6.6	4.9	0
4	South Kenai Beach	2.1	2.3	1.8	2.5	1.0	1.8	2.5	1.5	1.3	2.4	0.5	0	0	2.4	2.6	0
5	Kenai Boat Launch	2.5	2.3	2.9	4.4	2.5	3.2	4.4	2.9	2.8	4.3	1.2	1.2	0	3.6	3.6	0
6	Copper River Seafoods	1.6	1.2	1.7	2.8	1.1	1.7	2.6	1.6	1.4	2.7	0.6	0.6	0	1.9	1.6	0
7	Kenai River	4.5	3.9	3.4	5.1	3.1	4.3	4.8	4.1	3.8	5.0	2.7	3.3	1.2	3.8	3.3	1.2
8	Sewer Treatment Plant	0	0	0	2	0	0	2.2	0	0	2.0	0	0	0	2.9	2.1	0
9	Marathon Corporation	0	0	0	0	0	0	0	0	0	0	0	0	0	0	0	0
10	Offshore Systems	0	0	1.2	1.5	0.9	1.5	1.6	1.4	0	1.5	0	0	0	1.8	4.0	0

APPENDIX C: NINILCHIK
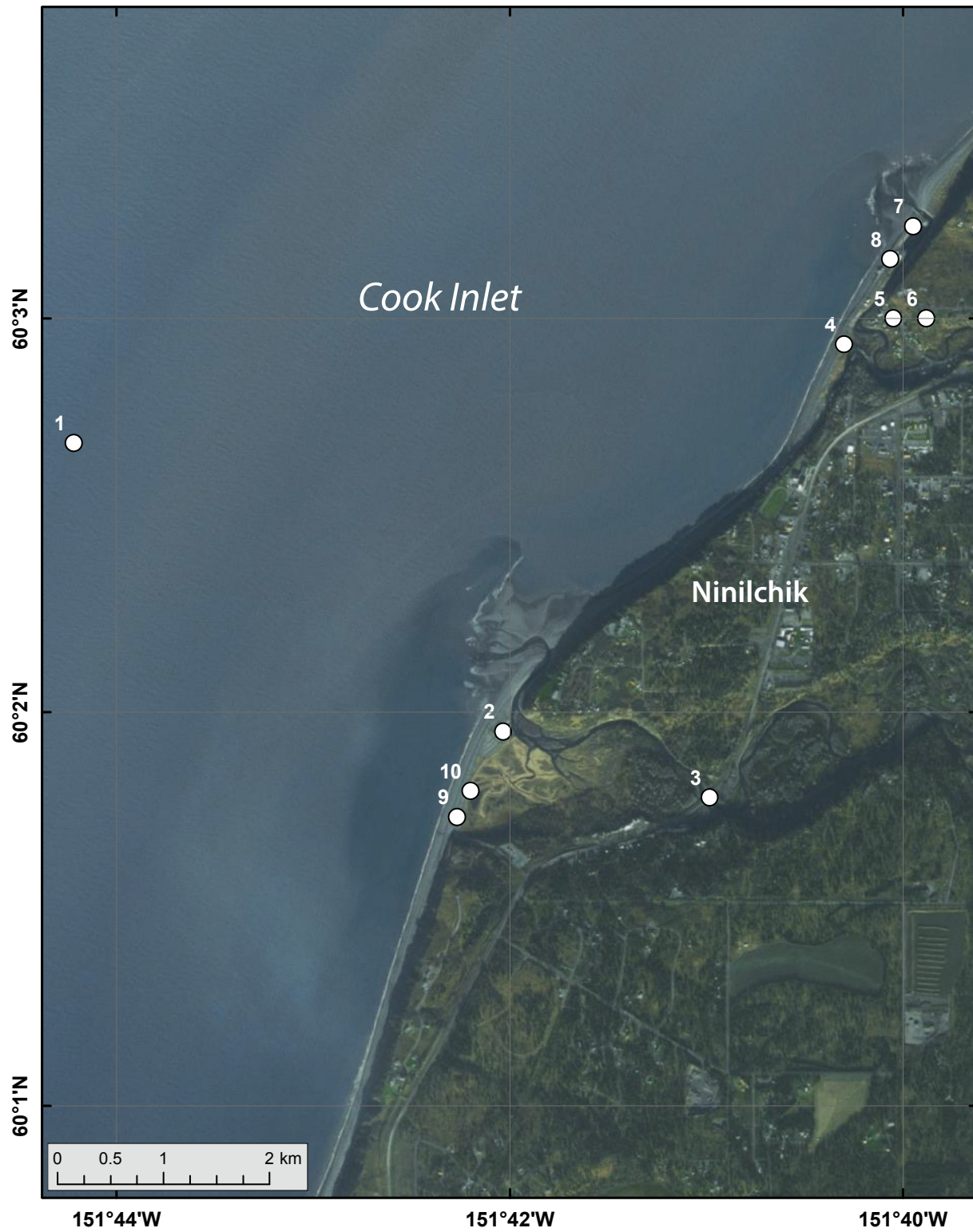
Figure C1. Locations of time series points in and around Ninilchik. The longitude and latitude locations of the time series points are listed in table C1.
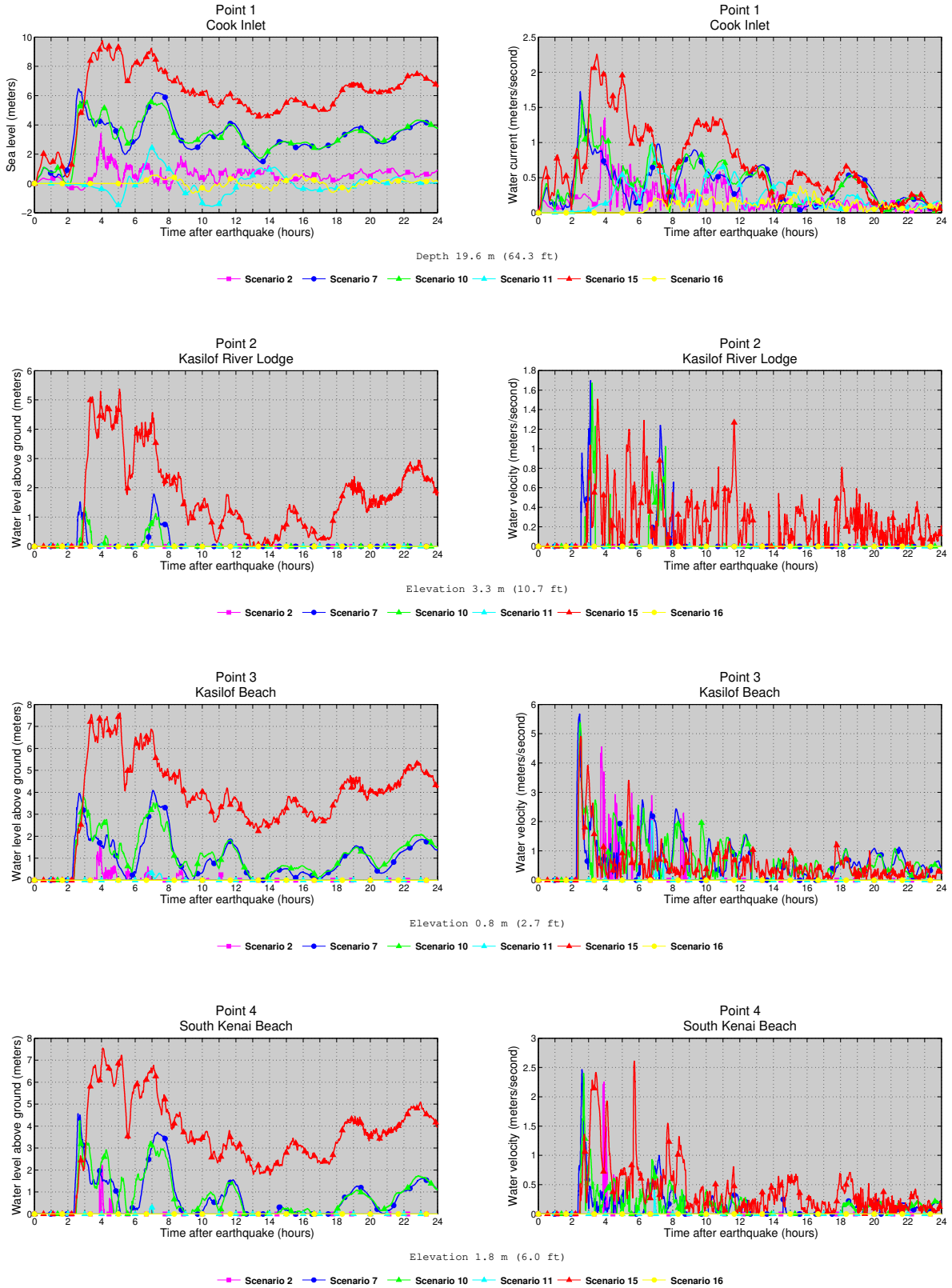
Figure C2. Time series of water level (left column) and velocity (right column) for selected scenarios at locations shown in figure C1. Elevations of onshore locations and ocean depth at offshore locations are given based on the pre-earthquake MHHW datum.
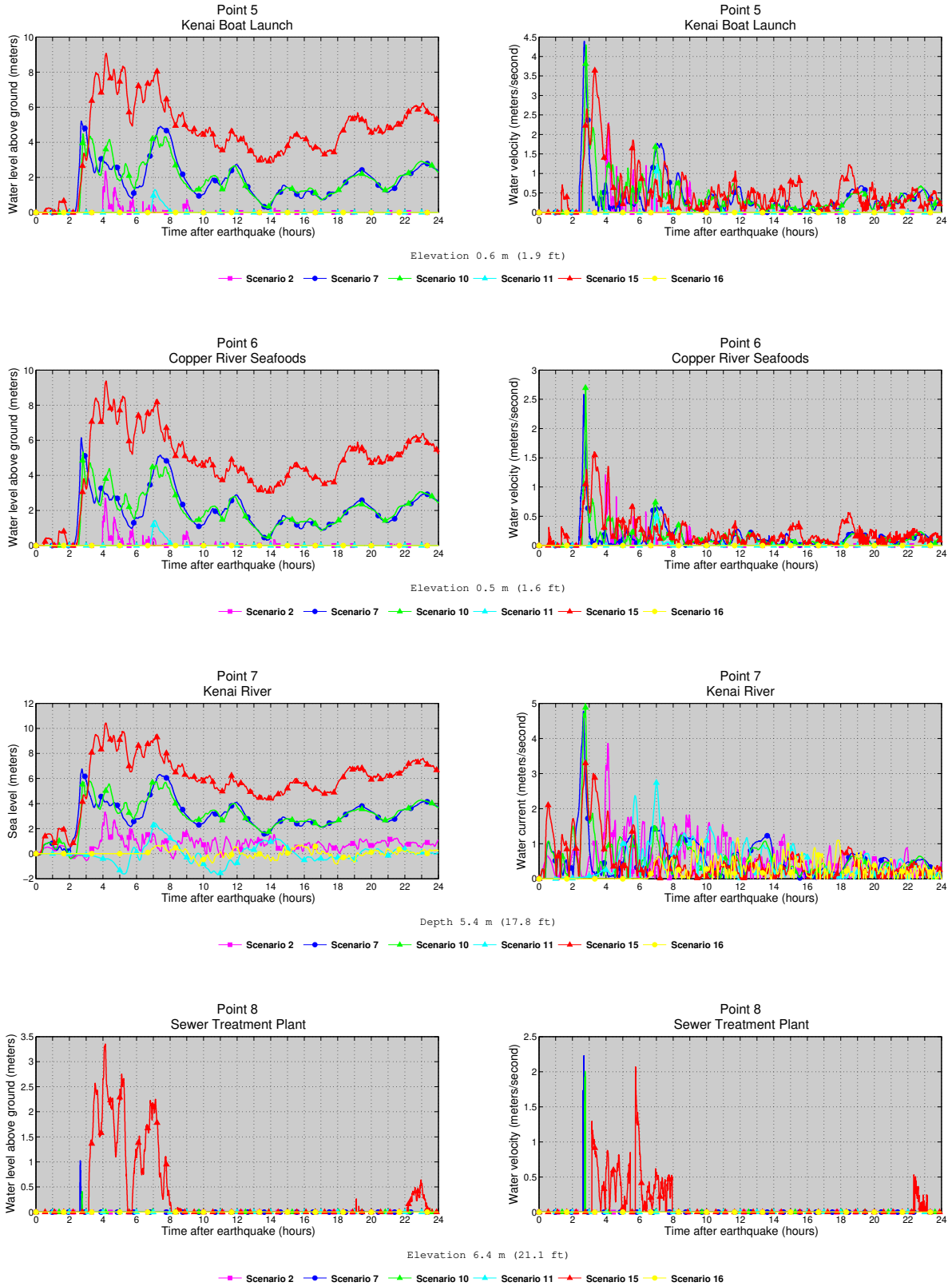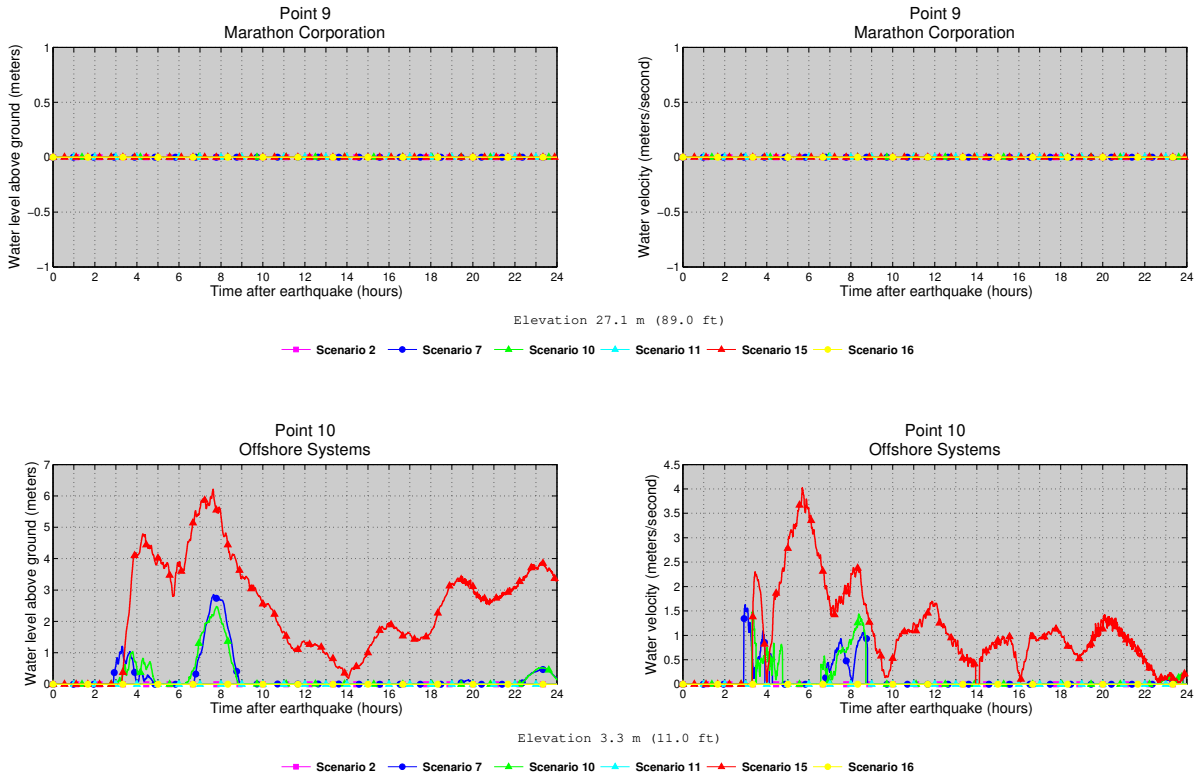
Figure C2, continued. Time series of water level (left column) and velocity (right column) for selected scenarios at locations shown in figure C1. Elevations of onshore locations and ocean depth at offshore locations are given based on the pre-earthquake MHHW datum.

Figure C2, continued. Time series of water level (left column) and velocity (right column) for selected scenarios at locations shown in figure C1. Elevations of onshore locations and ocean depth at offshore locations are given based on the pre-earthquake MHHW datum.

Table C1. Location of time series points in and around Ninilchik. The maximum water depth above ground is provided for onshore locations (S), whereas the maximum water level above the pre-earthquake MHHW is provided for offshore (O) locations.

#	Label	S/O	Longitude (°W)	Latitude (°N)	Min. elevation/ depth (m)
1	Cook Inlet	O	-151.736944	60.044722	23.4
2	Deep Creek Recreation	S	-151.700556	60.0325	-3.7
3	Sterling Hwy	S	-151.683056	60.029722	-2.0
4	Ninilchik Beach	S	-151.671667	60.048889	-4.3
5	Beach Access Road	S	-151.6675	60.05	-2.7
6	Russian Cemetery	S	-151.664722	60.05	22.4
7	Small Boat Harbor	O	-151.665833	60.053889	0.5
8	Airport Lane	S	-151.667778	60.0525	-3.6
9	Marine Services	S	-151.704444	60.028889	-3.8
10	Deep Creek Way	S	-151.703333	60.03	-4.1

Table C2. Maximum water depth for all tsunami scenarios at time series points in and around Ninilchik.

#	Label	Maximum water depth above ground/sea level (meters)															
		Scenario															
		1	2	3	4	5	6	7	8	9	10	11	12	13	14	15	16
1	Cook Inlet	3.2	3.4	5.4	5.8	5.5	6.2	6.5	6.1	4.1	5.7	2.4	2.3	1.1	6.9	9.8	0.7
2	Deep Creek Recreation	0	0	0.8	1.3	0.8	2.0	1.8	1.9	1.4	1.3	0	0	0	3.8	5.4	0
3	Sterling Hwy	1.4	1.6	3.2	3.8	3.2	4.1	4.1	4.2	3.5	3.8	0.4	0.3	0	5.8	7.6	0
4	Ninilchik Beach	3.0	2.2	3.5	4.5	3.0	3.9	4.6	3.8	2.4	4.2	0.4	0.2	0	5.6	7.6	0
5	Beach Access Road	2.4	2.4	4.2	4.7	4.2	5.1	5.2	5.0	3.3	4.5	1.3	1.0	0	6.6	9.1	0
6	Russian Cemetery	2.8	2.7	4.6	5.6	4.5	5.4	6.1	5.2	3.6	5.3	1.4	1.1	0	7.2	9.4	0
7	Small Boat Harbor	3.2	3.3	5.5	5.9	5.6	6.5	6.8	6.4	4.5	5.8	2.5	2.1	1.1	7.9	10.4	0.7
8	Airport Lane	0	0	0	0.7	0	0	1.0	0	0	0.4	0	0	0	1.4	3.4	0
9	Marine Services	0	0	0	0	0	0	0	0	0	0	0	0	0	0	0	0
10	Deep Creek Way	0	0	1.0	2.4	1.7	1.8	2.9	2.3	0	2.5	0	0	0	1.5	6.2	0

Table C3. Maximum water velocities for all tsunami scenarios at time series points in and around Ninilchik.

| #	Label	Maximum water velocity (meters/second)															
		Scenario															
		1	2	3	4	5	6	7	8	9	10	11	12	13	14	15	16
1	Cook Inlet	2.9	2.6	2.2	2.3	2.0	2.6	2.3	2.2	1.6	2.3	1.3	1.1	0.5	3.8	3.7	0.5
2	Deep Creek Recreation	6.9	6.6	4.8	3.5	1.6	3.8	2.8	1.5	1.6	3.3	0	0	0	8.2	3.5	0
3	Sterling Hwy	3.0	3.0	2.9	1.1	0.4	2.4	0.7	0.9	0.5	1.1	0	0	0	5.7	3.8	0
4	Ninilchik Beach	6.9	7.1	2.1	2.3	1.2	1.5	1.5	1.3	1.1	2.2	0	0	0	5.6	1.7	0
5	Beach Access Road	6.2	6.4	0.9	0.6	0.1	0.5	0.3	0.4	0.3	0.6	0	0	0	4.0	0.9	0
6	Russian Cemetery	0	0	0	0	0	0	0	0	0	0	0	0	0	0	0	0
7	Small Boat Harbor	11.7	11.6	1.3	1.4	0.8	1.1	0.9	0.7	0.7	1.4	0.4	0.3	0.1	4.0	1.4	0.1
8	Airport Lane	6.9	6.4	2.4	2.8	1.4	2.2	2.4	1.9	1.7	2.8	0	0	0	6.0	2.0	0
9	Marine Services	9.7	9.9	3.7	2.4	1.7	2.6	2.1	1.7	1.8	2.3	0	0	0	11	3.0	0
10	Deep Creek Way	7.5	7.2	5.7	4.8	3.9	5.0	4.5	3.3	3.9	4.6	0	0	0	8.3	4.8	0

APPENDIX D: TYONEK

Figure D1. Locations of time series points in and around Tyonek. The longitude and latitude locations of the time series points are listed in table D1.
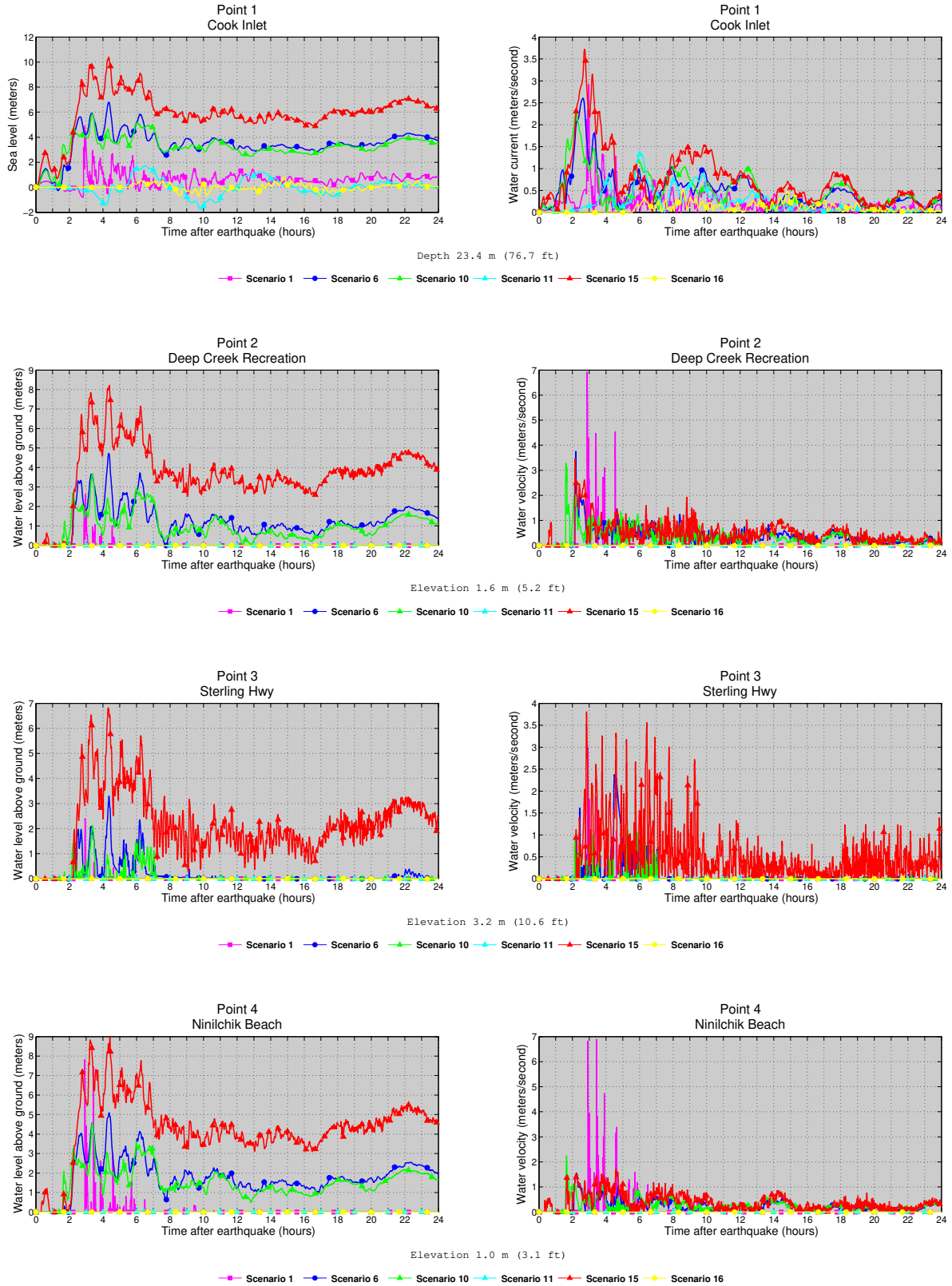
Figure D2. Time series of water level (left column) and velocity (right column) for selected scenarios at locations shown in figure D1. Elevations of onshore locations and ocean depth at offshore locations are given based on the pre-earthquake MHHW datum.
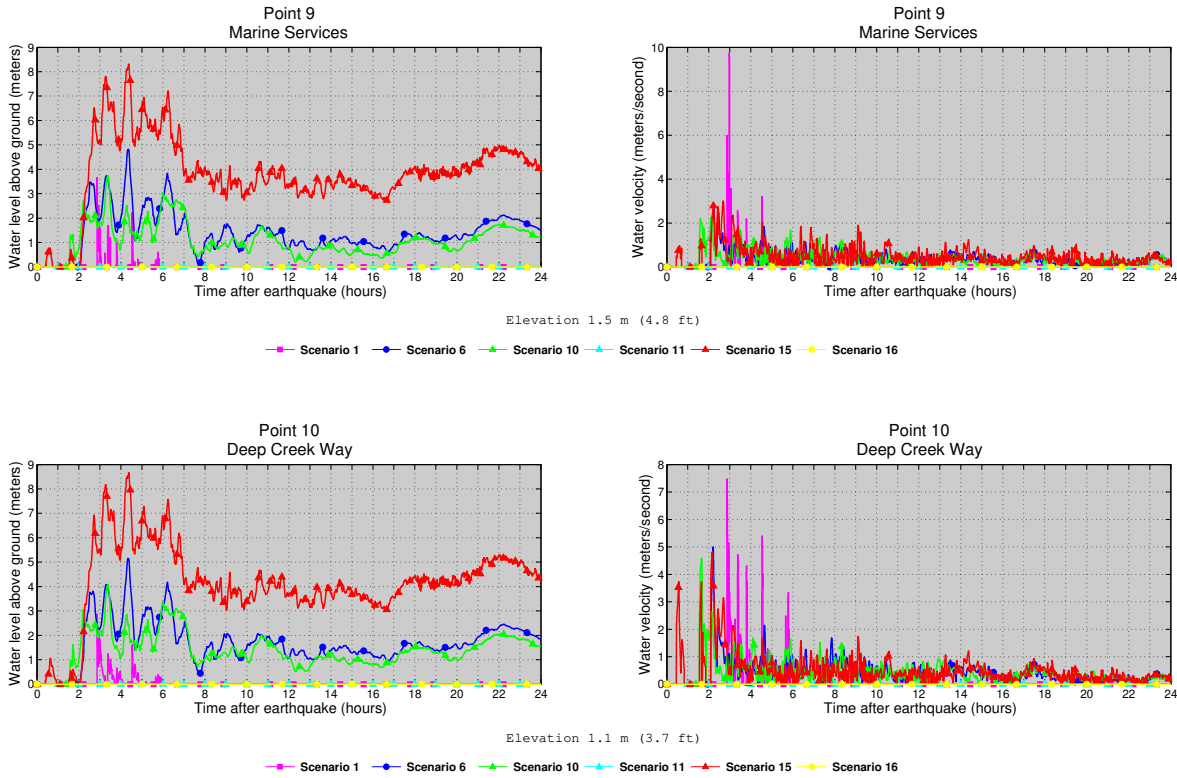
Figure D2, continued. Time series of water level (left column) and velocity (right column) for selected scenarios at locations shown in figure D1. Elevations of onshore locations and ocean depth at offshore locations are given based on the pre-earthquake MHHW datum.

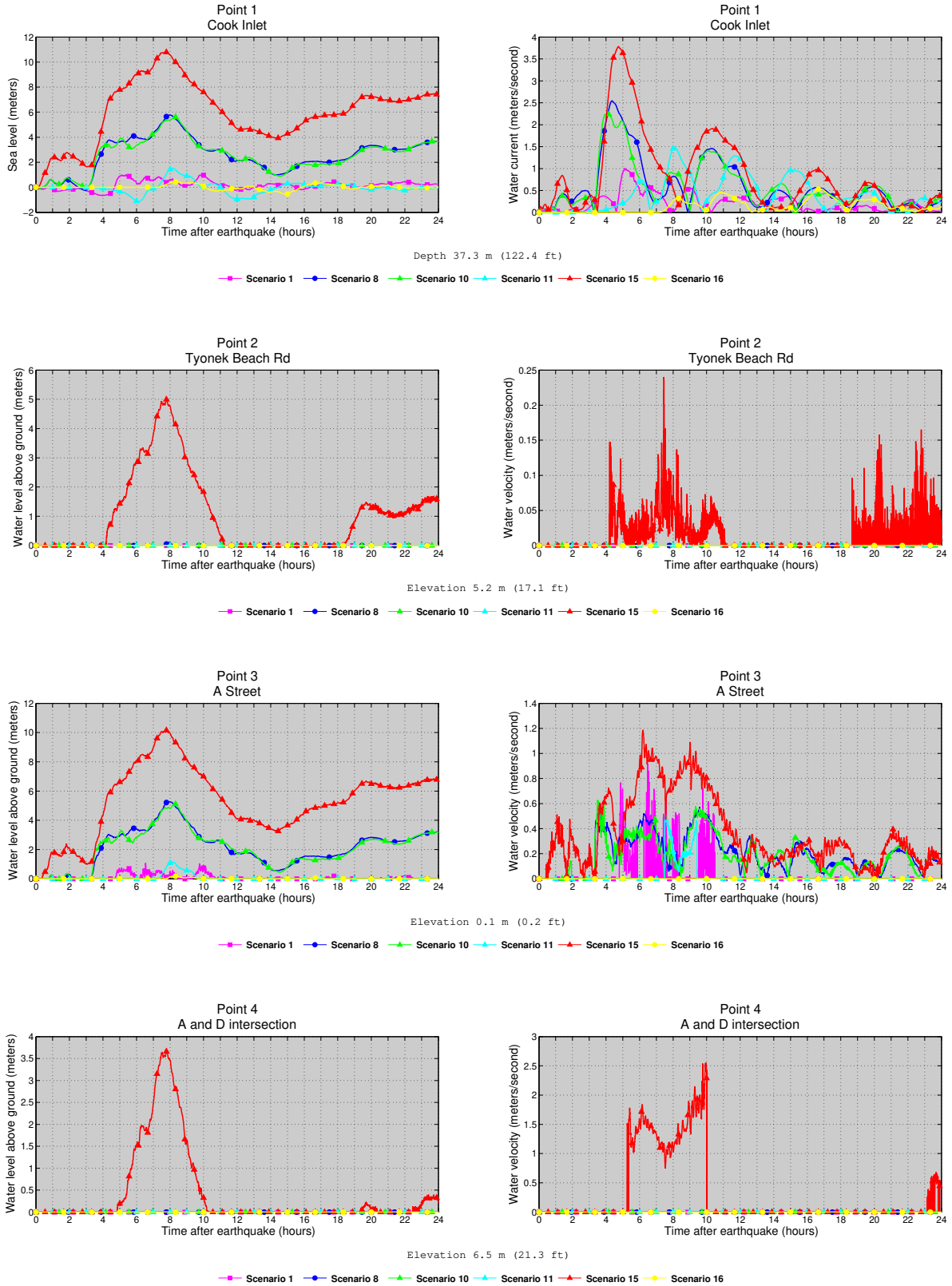**Figure D2, continued.** Time series of water level (left column) and velocity (right column) for selected scenarios at locations shown in figure D1. Elevations of onshore locations and ocean depth at offshore locations are given based on the pre-earthquake MHHW datum.
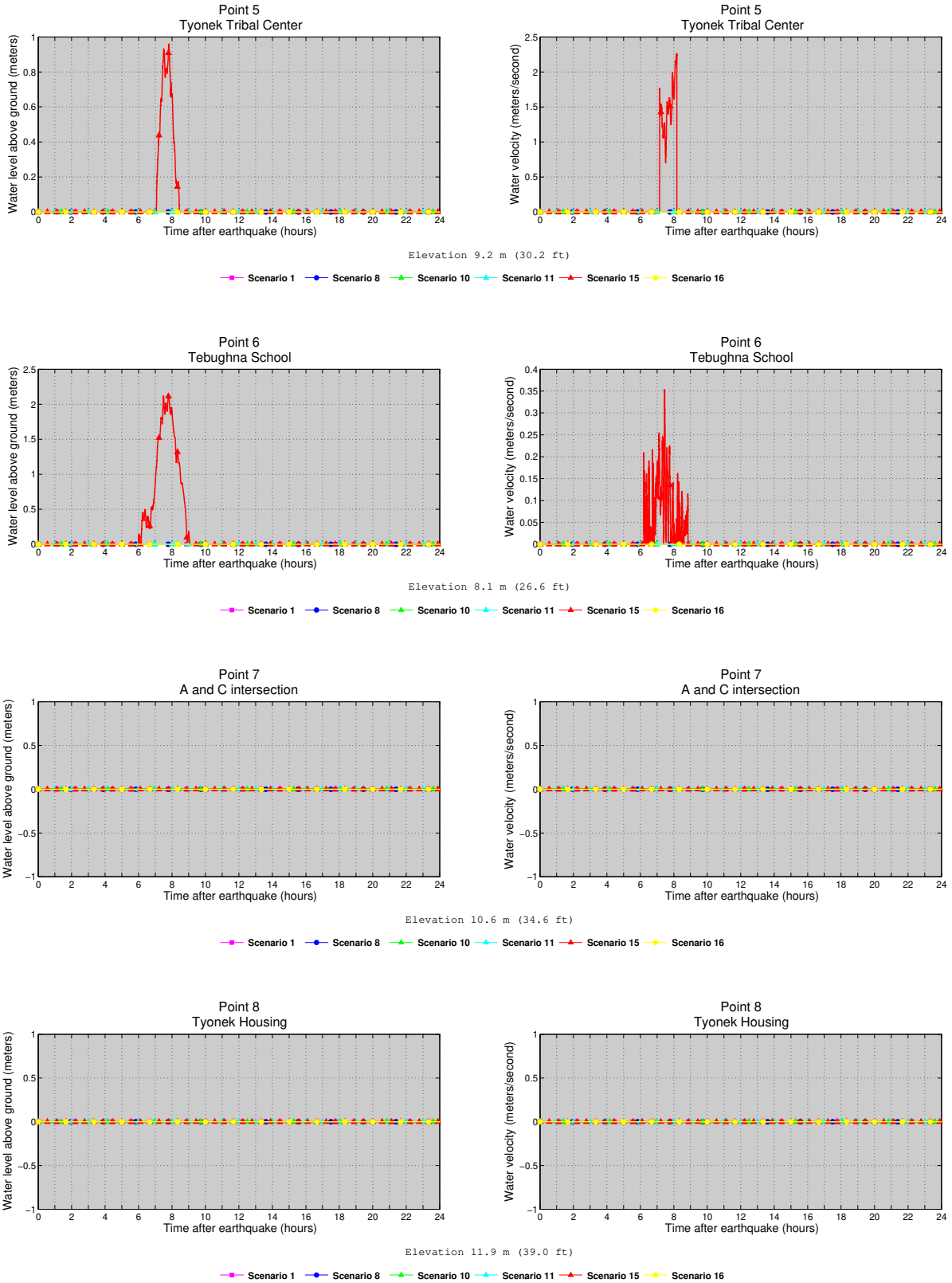
Table D1. Location of time series points in and around Tyonek. The maximum water depth above ground is provided for onshore locations (S), whereas the maximum water level above the pre-earthquake MHHW is provided for offshore (O) locations.

#	Label	S / O	Longitude (°W)	Latitude (°N)	Min. elevation/ depth (m)
1	Cook Inlet	O	-151.051667	61.048333	37.3
2	Tyonek Beach Rd	S	-151.146944	61.065278	-0.4
3	A Street	S	-151.141111	61.064722	-5.6
4	A and D intersection	S	-151.139722	61.065833	0.9
5	Tyonek Tribal Center	S	-151.139444	61.066389	3.6
6	Tebughna School	S	-151.144167	61.068056	2.5
7	A and C intersection	S	-151.138611	61.066944	4.9
8	Tyonek Housing	S	-151.136667	61.068056	6.2
9	Cottonwood Beach	O	-151.015278	61.183611	0.7
10	Store Road	S	-151.021667	61.180556	-4.4

Table D2. Maximum water depth for all tsunami scenarios at time series points in and around Tyonek.

#	Label	Maximum water depth above ground/sea level (meters)															
		Scenario															
		1	2	3	4	5	6	7	8	9	10	11	12	13	14	15	16
1	Cook Inlet	1.0	1.1	4.8	5.6	4.8	5.7	5.7	5.8	2.6	5.6	1.5	1.3	0.6	4.7	10.8	0.4
2	Tyonek Beach Rd	0	0	0	0	0	0	0.1	0.1	0	0	0	0	0	0	5.0	0
3	A Street	1.1	0.9	4.4	5.1	4.3	5.2	5.2	5.3	2.3	5.2	1.1	1.0	0.4	4.2	10.2	0.2
4	A and D intersection	0	0	0	0	0	0	0	0	0	0	0	0	0	0	3.7	0
5	Tyonek Tribal Center	0	0	0	0	0	0	0	0	0	0	0	0	0	0	1.0	0
6	Tebughna School	0	0	0	0	0	0	0	0	0	0	0	0	0	0	2.1	0
7	A and C intersection	0	0	0	0	0	0	0	0	0	0	0	0	0	0	0	0
8	Tyonek Housing	0	0	0	0	0	0	0	0	0	0	0	0	0	0	0	0
9	Cottonwood Beach	1.2	1.3	4.4	5.1	4.5	5.3	5.3	5.3	2.4	5.1	1.7	1.5	0.7	4.5	10.6	0.5
10	Store Road	0	0	3.0	3.7	3.0	3.9	3.8	3.8	0.9	3.7	0.3	0.1	0	3.1	9.1	0

Table D3. Maximum water velocities for all tsunami scenarios at time series points in and around Tyonek.

#	Label	Maximum water velocity (meters/second)															
		Scenario															
		1	2	3	4	5	6	7	8	9	10	11	12	13	14	15	16
1	Cook Inlet	1.0	1.1	1.8	2.2	2.0	2.7	2.4	2.5	1.4	2.2	1.5	1.2	0.6	2.2	3.8	0.5
2	Tyonek Beach Rd	0	0	0	0	0	0	0	0	0	0	0	0	0	0	0.2	0
3	A Street	0.9	0.8	0.5	0.6	0.5	0.7	0.6	0.6	0.6	0.6	0.5	0.6	0.3	0.6	1.2	0
4	A and D intersection	0	0	0	0	0	0	0	0	0	0	0	0	0	0	2.5	0
5	Tyonek Tribal Center	0	0	0	0	0	0	0	0	0	0	0	0	0	0	2.3	0
6	Tebughna School	0	0	0	0	0	0	0	0	0	0	0	0	0	0	0.4	0
7	A and C intersection	0	0	0	0	0	0	0	0	0	0	0	0	0	0	0	0
8	Tyonek Housing	0	0	0	0	0	0	0	0	0	0	0	0	0	0	0	0
9	Cottonwood Beach	1.5	1.2	2.0	2.0	1.9	2.4	2.0	2.0	1.7	2.0	1.6	1.7	0.9	2.1	2.4	0.9
10	Store Road	0	0	0.6	0.9	0.6	0.8	0.8	0.6	0.3	0.9	0	0	0	0.7	1.3	0